Novel Sterically Crowded and Conformationally Constrained α-Aminophosphonates with a Near-Neutral pKa as Highly Accurate 31 P NMR pH Probes. Application to Subtle pH Gradients Determination in Dictyostelium discoideum Cells

Caroline Delehedde, Marcel Culcasi, Emilie Ricquebourg, Mathieu Cassien, Didier Siri, Bruno Blaive, Sylvia Pietri, Sophie A.L. Thétiot-Laurent

molecules

MDPI

Article

Novel Sterically Crowded and Conformationally Constrained α-Aminophosphonates with a Near-Neutral pK_a as Highly Accurate ^{31}P NMR pH Probes. Application to Subtle pH Gradients Determination in *Dictyostelium discoideum* Cells

Caroline Delehedde [1], Marcel Culcasi [1], Emilie Ricquebourg [1], Mathieu Cassien [2], Didier Siri [3], Bruno Blaive [1], Sylvia Pietri [1] and Sophie Thétiot-Laurent [1,*]

[1] Aix Marseille Univ, CNRS, ICR, UMR 7273, SMBSO, 13397 Marseille, France; caroline.delehedde@etu.univ-amu.fr (C.D.); marcel.culcasi@cnrs.fr (M.C.); emilie.ricquebourg@laposte.net (E.R.); bruno.blaive@univ-amu.fr (B.B.); sylvia.pietri@univ-amu.fr (S.P.)
[2] Yelen Analytics, 10 Boulevard Tempête, 13820 Ensuès-la-Redonne, France; mathieu.cassien@yelen-analytics.com
[3] Aix Marseille Univ, CNRS, ICR, UMR 7273, CT, 13397 Marseille, France; didier.siri@univ-amu.fr
* Correspondence: sophie.thetiot-laurent@univ-amu.fr; Tel.: +33-(0)4-13-94-58-07

Abstract: In order to discover new ^{31}P NMR markers for probing subtle pH changes (<0.2 pH unit) in biological environments, fifteen new conformationally constrained or sterically hindered α-aminophosphonates derived from diethyl(2-methylpyrrolidin-2-yl)phosphonate were synthesized and tested for their pH reporting and cytotoxic properties in vitro. All compounds showed near-neutral pK_as (ranging 6.28–6.97), chemical shifts not overlapping those of phosphorus metabolites, and spectroscopic sensitivities (i.e., chemical shifts variation $\Delta\delta_{ab}$ between the acidic and basic forms) ranging from 9.2–10.7 ppm, being fourfold larger than conventional endogenous markers such as inorganic phosphate. X-ray crystallographic studies combined with predictive empirical relationships and ab initio calculations addressed the inductive and stereochemical effects of substituents linked to the protonated amine function. Satisfactory correlations were established between pK_as and both the 2D structure and pyramidalization at phosphorus, showing that steric crowding around the phosphorus is crucial for modulating $\Delta\delta_{ab}$. Finally, the hit ^{31}P NMR pH probe **1b** bearing an unsubstituted 1,3,2-dioxaphosphorinane ring, which is moderately lipophilic, nontoxic on A549 and NHLF cells, and showing pK_a = 6.45 with $\Delta\delta_{ab}$ = 10.64 ppm, allowed the first clear-cut evidence of trans-sarcolemmal pH gradients in normoxic *Dictyostelium discoideum* cells with an accuracy of <0.05 pH units.

Keywords: α-aminophosphonates; pH probes; ^{31}P NMR; phophorus pyramidalization angle; X-ray crystallography; trans-sarcolemmal pH gradients; *Dictyostelium discoideum* cells

Citation: Delehedde, C.; Culcasi, M.; Ricquebourg, E.; Cassien, M.; Siri, D.; Blaive, B.; Pietri, S.; Thétiot-Laurent, S. Novel Sterically Crowded and Conformationally Constrained α-Aminophosphonates with a Near-Neutral pK_a as Highly Accurate ^{31}P NMR pH Probes. Application to Subtle pH Gradients Determination in *Dictyostelium discoideum* Cells. *Molecules* **2022**, *27*, 4506. https://doi.org/10.3390/molecules27144506

Academic Editor: Marilisa Leone

Received: 21 May 2022
Accepted: 12 July 2022
Published: 14 July 2022

1. Introduction

Intracellular (cytosolic) pH (pH_i) is a fundamental physiological parameter whose changes affect nearly all metabolic and growth/proliferation cellular processes, and can also occur in response to exogenous agents. Maintaining pH homeostasis in the cytosol, extracellular milieu (pH_e) and subcellular compartments (such as lysosomes, mitochondria, and endosomal vesicles) is crucial for all living organisms. Among the mechanisms of pH_i regulation, the Na^+/H^+ antiporter represents a major pathway for the exit of protons from cells during acidification and the entry of Na^+ from the extracellular medium to balance the net charge movement [1]. Indeed, pH_i and pH_e are in a dynamic steady state and, in normal mammalian cells, pH_i is close to neutrality (~7.2) while pH_e is slightly alkaline

(ranging 7.3–7.5) [1]. Therefore, experimentally assessing pH regulation in pathological situations requires both pH_i and pH_e to be monitored simultaneously and accurately.

Since Moon and Richard's first report [2], ^{31}P nuclear magnetic resonance (NMR) has become a powerful and non-invasive technique for determining pH_i on the basis of the variation of pH, with the chemical shift of endogenous inorganic phosphate (PO_4^{3-}; P_i) [3–8]. This technique has been applied to a variety of biological systems, e.g., for monitoring bioenergetics and/or the metabolism of various organs [9–15]. ^{31}P NMR is also routinely used in the study of food chemistry, quality, and safety control [16,17] or for monitoring the production of everyday products [18], to name but a few. Despite P_i being ubiquitous in cells, its use as an 'universal' ^{31}P NMR pH sensor in biological studies has, however, many drawbacks that may impair spectroscopic detection. First, given that the absolute value of the chemical shift difference between the protonated acidic (δ_a) and unprotonated basic (δ_b) forms of P_i ($\Delta\delta_{ab} = |\delta_a - \delta_b|$) is only ~2.6 ppm, with a pK_a ~6.75 (for its second acidity [19]), it cannot sense pH_i/pH_e differences of less than 0.3 pH units [2]. Moreover, the fluctuations of P_i concentration during metabolism and its low availability in the extracellular space and many organelles considerably hinder direct access to local pH measurements using this probe [20]. Ideally, the structural requirements for improved ^{31}P NMR pH markers would both involve (i) increasing $\Delta\delta_{ab}$ as to get pH titration curves with the steepest slope around the pK_a value and (ii) modulating the pK_a value(s) to fine tune extracellular/intracellular pH domains of interest.

In order to minimize the possible cytotoxic effects, the first synthetic attempts towards these above conditions focused on modifications around the P_i structure to get alkylated phosphonic acids RP(O)$(OH)_2$ (Figure 1A), which were found to exhibit slightly increased $\Delta\delta_{ab}$ values and pK_as of 7.0 ± 0.5 [21]. To illustrate, the methylphosphonate pK_a = 7.36, with $\Delta\delta_{ab}$ = 3.88 ppm at 20 °C in a Krebs–Henseleit (KH) buffer is currently used in organ perfusion experiments [19]. Further targets were α-, β- and γ-substituted linear aminophosphonic acids (Figure 1B) whose $\Delta\delta_{ab}$ values, however, did not exceed 3.4 ppm [22], but showed relatively weak toxicity and had lower pK_as suitable for probing the acidic domains in cells, tumors, and perfused organs [23–26]. Since in all these above compounds, protonation always occurs at the phosphorus first, it was then speculated that scaffolds bearing a non-ionizable *P*-atom (e.g., a phosphonate) and a protonable α-amino group (typically, a secondary amine) would offer considerable advantages in terms of $\Delta\delta_{ab}$ and pK_a modulation due to different inductive and steric effects. This approach led to the development of two families of uncharged pH probes, including cyclic pyrrolidine-based α-aminophosphonates (Figure 1C) and linear polysubstituded α-aminophosphonates (Figure 1D) [19,27–31]. For all these compounds, it was found that protonation, which gives the ammonium salt as the acidic species, resulted in lower pK_as and gave $\Delta\delta_{ab}$ values up to fourfold greater than that of P_i or phosphonic acids. Thus, the reported pH titration curves for the α-aminophosphonate having the structure shown in Figure 1D, with {R_1 = R_2 = R_3 = Me; R_4 = Et; R_5 = Me; R_6 = H} afforded $\Delta\delta_{ab}$ = 10.3 ppm and pK_a = 7.01 in KH buffer [28]. Later, the successful mitochondrial targeting of selected compounds shown in Figure 1D was achieved by grafting a triphenylphosphonium cation (Figure 1E), and most of the resulting structures retained the good pH-probing performance of their parent compounds [32,33]. To illustrate, using a nontoxic micromolar concentration of the triphenylphosphonium bromide having the structure shown in Figure 1E (right part) with {R_1 = R_2 = H; R_3 = R_4 = Me; n = 7}, for which $\Delta\delta_{ab}$ = 10.3 ppm and pK_a = 6.99, allowed the first ^{31}P NMR assessment of acidic and cytosolic mitochondrial compartments of the green alga *Chlamydomonas reinhardtii* [33].

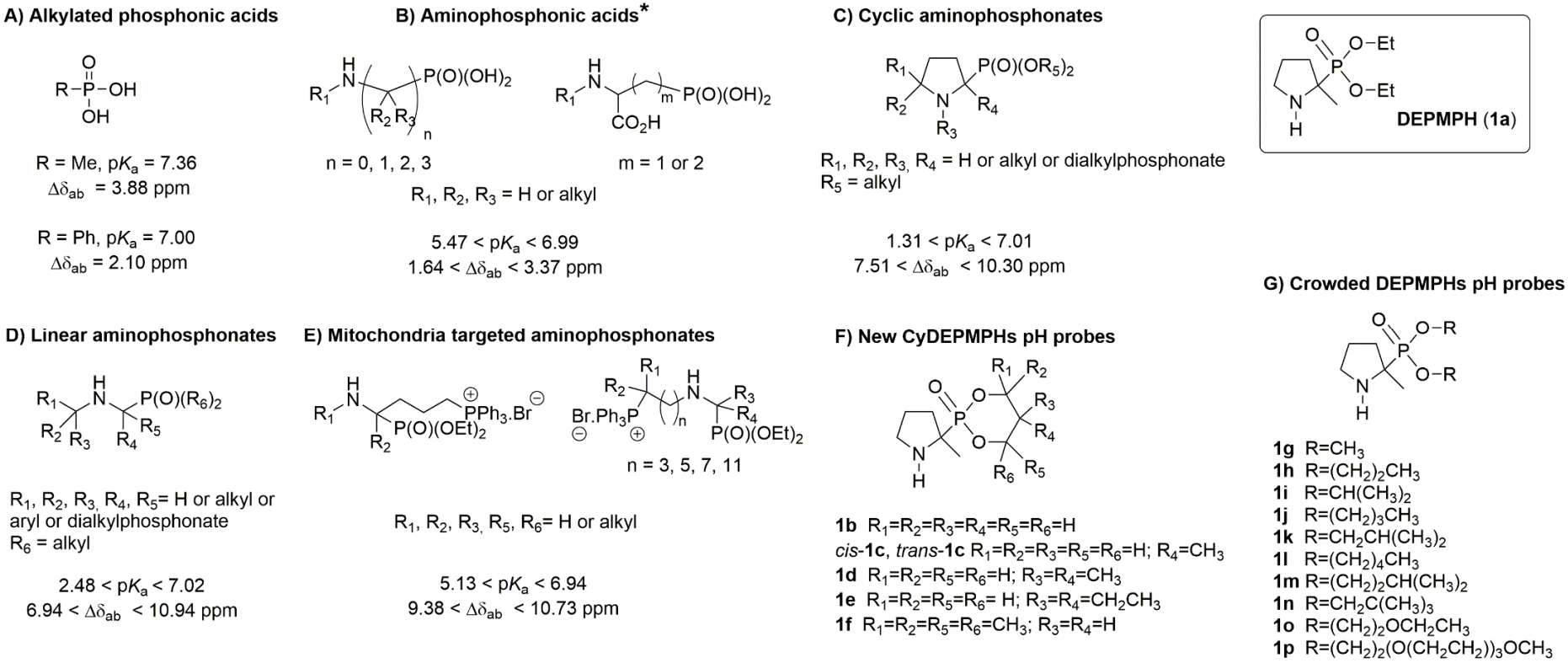

Figure 1. (**A**–**E**) Families of phosphorylated derivatives used as exogenous ^{31}P NMR pH probes. (**F**) Conformationally constrained CyDEPMPHs pH probes (current study). (**G**) Sterically crowded DEPMPH-derived pH probes (current study). *Inset*: Structure of DEPMPH (**1a**). * pK_a and $\Delta\delta_{ab}$ values of the second OH of phosphonic group.

The knowledge of small trans-sarcolemmal pH gradients is one of the most important pieces of dynamic information to be obtained using very sensitive pH probes, especially when the external P_i peak is hardly or not detectable [34]. This was addressed in normoxic perfused rat hearts either by ^{31}P NMR with the cell impermeable phenylphosphonic acid (Figure 1A; R = Ph) [34] or by ^{19}F NMR using a fluorinated pyridine derivative [35], and in these early studies, reachable trans-sarcolemmal gradients were found to be 0.24 and 0.38 pH units, respectively. Based on their significantly larger $\Delta\delta_{ab}$s when compared to, e.g., phenylphosphonic acid (having pK_a = 7.00 and $\Delta\delta_{ab}$ = 2.10 ppm; Figure 1A [21]), many newer ^{31}P NMR pH probes displayed in Figure 1C,D could be much better alternatives in probing more subtle pH changes (<0.2 pH units) occurring in acidotic cells. Actually, such an improvement was obtained using diethyl(2-methylpyrrolidin-2-yl)phosphonate **1a** (DEPMPH, having pK_a = 7.01 and $\Delta\delta_{ab}$ = 9.77 ppm [19]; see Figure 1 inset) during ischemia of the rat isolated heart or liver [27]. However, despite the given advantage to probe the intra, extra and acidic regions simultaneously, **1a** was found to be less accurate than P_i for cytosolic pH determination [27]. The line width broadening at pH ≈ pK_a impairs any accurate pH determination [29], therefore excluding probes having a pK_a close to the pH region of interest. Moreover, the strictly neutral pK_a of **1a** was a drawback for assessing accurately the pH variations in acidic compartments [27]. It can therefore be inferred that, besides a $\Delta\delta_{ab}$ value > 10 ppm, a better differentiation between the intracellular vs. extracellular NMR peaks would demand shifting of the pK_a of the probe downwards to, e.g., 6.2–6.8.

Previously a semi-empirical linear model was established for predicting the pK_a of **1a** and derivatives based on their 2D geometries and the additive inductive effect of substituents in β position of the nitrogen (e.g., R_1–R_5 and the phosphonyl group in Figure 1D) [19]. In the present study the DEPMPH pyrrolidine scaffold was used to elaborate novel derivatives in which the *P*-bound alkoxy groups were either constrained as a 2-oxo-1,3,2-dioxaphospharinane ring (CyDEPMPHs family **1b–f**; Figure 1F) or induced steric crowding around the *P*-atom (crowded family **1g–p**; Figure 1G). Compounds were investigated for their ^{31}P NMR relaxation properties and pH reporting behavior in vitro. The collected experimental $\Delta\delta_{ab}$ values and pK_as were found to be consistent inputs to consolidate the empirical relationships of [19]. Additional density functional theory (DFT) calculations were performed on the [C–P–O] pyramidalization angle of compounds **1a–p**, pooled with a large series of structurally related compounds. The results, together with structural complements using X-ray structures of those crystallized CyDEPMPHs, established a relationship between pyramidalization around P and $\Delta\delta_{ab}$. From the above parameters, experimentally determined cytotoxicities, and calculated lipophilicities, the hit compound **1b** was selected and its ability to simultaneously probe the intra, extra and acidic regions was checked in normoxic *Dictyostelium discoideum* cells. For the first time, a trans-membrane pH gradient with an estimated precision of < 0.05 pH units was found in full accordance with the pH values given by the cytosolic and external P_i peaks, suggesting that **1b** could be a useful tool in a pathological situation where P_i peaks fall below the NMR detection limit.

2. Results and Discussion

2.1. Chemistry and X-ray Crystallography

Aminophosphonates **1a–p** were synthesized according to the general sequence outlined in Scheme 1, involving the reaction of the corresponding dialkyl H-phosphonate **2a–p** with 2-methyl-1-pyrroline. Starting compounds dialkyl H-phosphonates **2a**, **2g**, **2i**, and **2j** are commercially available, while the other precursors **2b–f**, **h**, **k–p** were synthesized according to [36] with slight modifications. Briefly, H-phosphonic bis(dimethylamide) was prepared in situ by the addition of one equivalent of water to hexamethylphosphorous triamide (HMPT) in tetrahydrofuran (THF), and then alcohol was added to give the corresponding compounds **2b–f, h, k–p**. Reactions were monitored directly by ^{31}P NMR

by following the disappearance of HMPT peak (δ = 122.24 ppm) followed by the formation of bis(dimethylamino)phosphoric acid peak (δ = 24.0 ppm), then by the disappearance of this latter and the formation of the corresponding dialkyl H-phosphonate peak. Dialkyl (2-methylpyrrolidin-2-yl) phosphonates **1a**–**p** were obtained by the nucleophilic addition of dialkyl H-phosphonates **2a**–**p** onto 2-methyl-1-pyrroline in toluene [37] in good yields (49–73%).

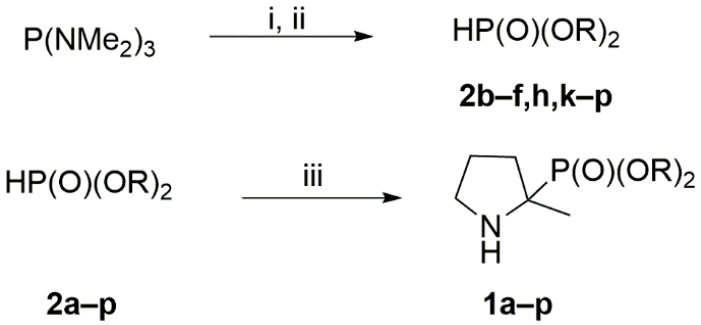

Scheme 1. General synthesis of aminophosphonates **1a**–**p**. Reagents and conditions: (i) 1 equiv H_2O, 3 h, 70 °C, THF; (ii) 1 equiv diol (series **b**–**f**), 6 h, 70 °C, THF or 2 equiv alcohol (series **h,k**–**p**), 3 h, 70 °C, THF; (iii) 1.1 equiv 2-methyl-1-pyrroline, 2 h–10 d, rt, toluene.

Single crystals suitable for X-ray diffraction analysis were obtained for the five compounds **1b**, *trans*-**1c**, and **1d**–**f** by recrystallization from a dichloromethane:*tert*-butylmethylether (TBME) mixture (Figure 2). The pyrroline rings were found to adopt puckered conformations which can be either the E + 4 (ϕ = 72°) envelope conformation (**1b**), the T1 (ϕ = 18°) twist conformation (*trans*-**1c**) or an intermediate situation between the T1 and E + 4 conformations (**1d**–**f**) according to the classification of [38]. The C–P bond is pseudo-axial in compounds **1e** and **1f** and pseudo-equatorial in compounds **1b**, *trans*-**1c**, and **1d** (Table 1), as referred to by the sign of the C(5)–N(1)–C(2)–C(3) dihedral angle in nitrones analogues of CyDEPMPHs [39].

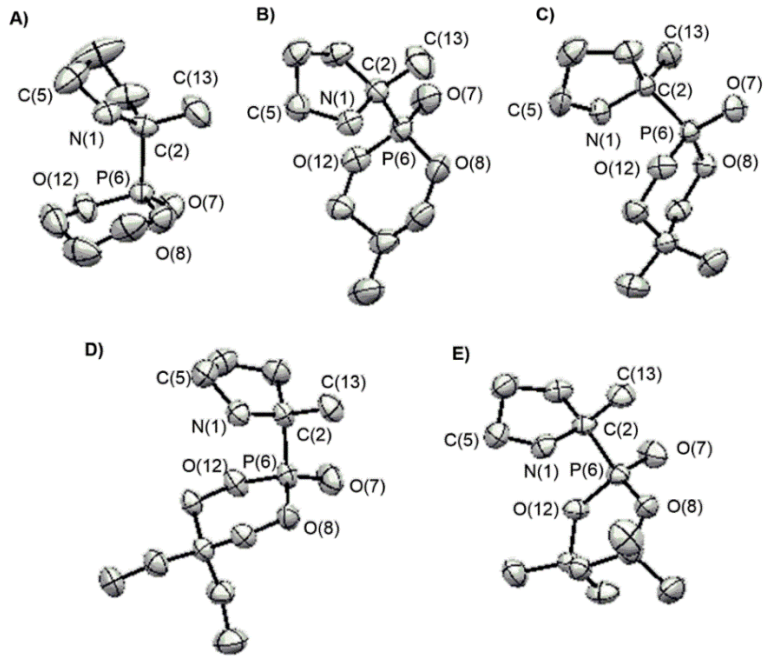

Figure 2. ORTEP drawings of CyDEPMPHs (**A**) **1b**; (**B**) *trans*-**1c**; (**C**) **1d**; (**D**) **1e**; (**E**) **1f** showing the labeling of atoms (see also Table 1 heading) and their displacement ellipsoids at the 40% probability level. For clarity, H-atoms have been omitted.

Table 1. General Structure, Atoms Numbering and Selected X-Ray Crystallographic Data of CyDEPMPHs [a].

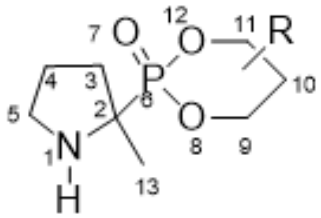

	1b	***trans*-1c**	**1d**	**1e**	**1f**
Bond length (Å)					
N(1)–H	0.941(0)	1.058(0)	1.053(0)	1.004(0)	0.990(0)
N(1)–C(2)	1.481(2)	1.482(3)	1.485(3)	1.482(3)	1.486(3)
N(1)–C(5)	1.463(4)	1.452(3)	1.478(3)	1.480(3)	1.461(3)
C(2)–P(6)	1.810(2)	1.813(2)	1.814(2)	1.826(2)	1.815(2)
P(6)–O(7)	1.466(2)	1.465(2)	1.462(2)	1.466(2)	1.465(2)
P(6)–O(8)	1.570(2)	1.579(2)	1.573(1)	1.578(2)	1.575(1)
P(6)–O(12)	1.576(2)	1.571(1)	1.579(1)	1.581(2)	1.561(2)
Distance length (Å)					
H–O(7)	4.559(1)	4.560(2)	4.589(0)	4.644(1)	4.658(1)
Bond angle (°)					
C(5)–N(1)–C(2)	108.1(2)	108.3(2)	106.4(2)	109.0(2)	106.7(2)
N(1)–C(2)–C(3)	105.7(2)	105.2(2)	106.7(1)	105.0(2)	106.1(2)
N(1)–C(2)–P(6)	107.9(1)	108.9(1)	108.6(1)	108.6(1)	110.0(2)
N(1)–C(2)–C(13)	111.7(2)	111.6(2)	110.5(1)	111.7(2)	110.6(2)
C(2)–P(6)–O(7)	112.9(1)	112.0(1)	112.3(9)	113.1(1)	111.5(1)
C(2)–P(6)–O(12)	107.5(9)	107.1(9)	107.4(8)	107.7(9)	109.1(1)
C(2)–P(6)–O(8)	106.9(9)	108.2(1)	1080(8)	107.7(9)	105.1(9)
C(13)–C(2)–P(6)	109.4(1)	110.0(2)	108.8(1)	108.4(1)	108.7(2)
Dihedral angle (°)					
C(5)–N(1)–C(2)–C(3)	−0.5(2)	−1.0(2)	−9.0(2)	0.4(2)	10.9(2)
C(5)–N(1)–C(2)–P(6)	117.7(2)	−117.9(2)	109.3(2)	−117.8(2)	106.7(2)

N(1)–C(2)–C(3)–C(4)	5.6(0)	24.1(2)	−12.3(2)	−20.2(2)	12.9(2)
H– N(1)–C(2)–P(6)	−122.6(2)	127.9(0)	−132.6(1)	138.8(1)	119.7(1)
N(1)–C(2)–P(6)–O(7)	−174.1(1)	175.8(1)	−175.8(1)	177.2(1)	170.8(1)
N(1)–C(2)–P(6)–O(12)	−92.2(0)	53.2(2)	−51.6(1)	53.9(1)	46.9(2)
N(1)–C(2)–P(6)–O(8)	7.87(1)	−60.4(2)	61.8(1)	−58.9(1)	−66.5(2)
C(13)–C(2)–P(6)–O(7)	64.2(2)	−61.5(2)	63.9(1)	−61.3(2)	−68.0(2)

[a] Values in parentheses are estimated standard deviations.

2.2. pH Dependent ^{31}P NMR Properties of New α-Aminophosphonates

The pH dependence of the ^{31}P NMR chemical shift of **1a–p** was investigated at 22 °C in KH buffer (pH 7.35). Monophasic acid–base titration curves reflecting protonation on nitrogen were obtained for all the derivatives (see examples in Figure 3) and their fitting to the Henderson–Hasselbalch equation (see Equation (2) in Materials and Methods) allowed the calculation of pK_as, the ^{31}P NMR parameters (δ_a, δ_b, and $\Delta\delta_{ab}$), and the spin lattice relaxation time (T_1) (Table 2).

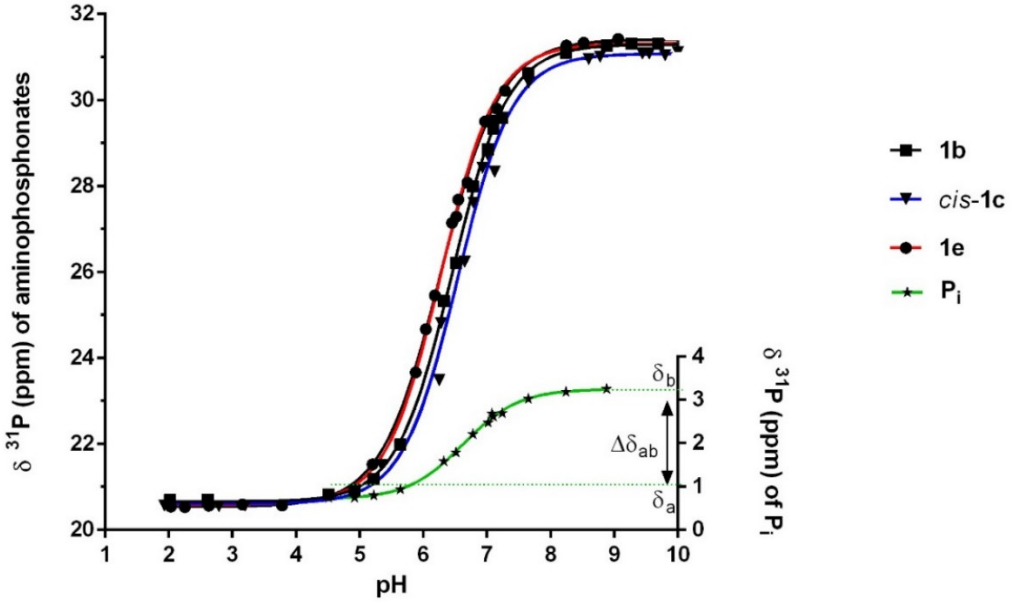

Figure 3. pH Dependence of the ^{31}P chemical shift of CyDEPMPHs **1b**, *cis*-**1c**, and **1e** compared to P_i. Titrations were performed at 22 °C in a modified KH buffer (pH 7.35) and each curve was obtained by the nonlinear fitting of 3–10 independent experiments. Outlined: limiting acidic (δ_a) and basic (δ_b) chemical shifts, and their difference ($\Delta\delta_{ab}$) for P_i.

Table 2. ^{31}P NMR Parameters and pK_a Values [a] in KH Medium at 22 °C.

Compounds	pK_a	δ_a (ppm)	δ_b (ppm)	$\Delta\delta_{ab}$ (ppm)	T_1 (s)
P_i	6.72 ± 0.11	0.81 ± 0.02	3.32 ± 0.03	2.51 ± 0.03	10.50
1a	7.01 ± 002	23.08 ± 0.06	32.85 ± 0.06	9.77 ± 0.11	5.40
CyDEPMPHs family					
1b	6.45 ± 0.01	20.65 ± 0.05	31.29 ± 0.04	10.64 ± 0.09	6.00
***trans*-1c**	6.45 ± 0.02	19.07 ± 0.11	29.95 ± 0.08	10.58 ± 0.19	5.11
***cis*-1c**	6.54 ± 0.03	20.60 ± 0.16	31.08 ± 0.12	10.48 ± 0.28	4.77
1d	6.22 ± 0.01	19.63 ± 0.08	30.33 ± 0.06	10.70 ± 0.14	4.51
1e	6.28 ± 0.01	20.58 ± 0.05	31.32 ± 0.05	10.74 ± 0.10	4.45
1f	6.79 ± 0.01	18.34 ± 0.03	27.69 ± 0.03	9.35 ± 0.06	4.06
Crowded family					
1g	6.70 ± 0.01	26.29 ± 0.05	35.89 ± 0.04	9.60 ± 0.09	7.96
1h	6.89 ± 0.01	23.85 ± 0.04	33.39 ± 0.04	9.55 ± 0.08	5.06
1i	6.97 ± 0.02	21.44 ± 0.10	31.30 ± 0.10	9.86 ± 0.20	4.70
1j	6.88 ± 0.01	23.85 ± 0.06	33.45 ± 0.05	9.60 ± 0.11	4.27
1k	6.78 ± 0.04	23.69 ± 0.20	33.03 ± 0.18	9.34 ± 0.38	4.16
1l	6.71 ± 0.01	23.78 ± 0.07	33.35 ± 0.07	9.57 ± 0.14	3.90
1m	6.76 ± 0.02	23.93 ± 0.10	33.37 ± 0.10	9.44 ± 0.20	3.62
1n	6.71 ± 0.01	23.57 ± 0.06	32.76 ± 0.06	9.19 ± 0.12	3.91

1o	6.62 ± 0.01	24.09 ± 0.07	33.88 ± 0.06	9.79 ± 0.13	3.75
1p	6.63 ± 0.01	24.10 ± 0.09	33.84 ± 0.07	9.74 ± 0.16	2.64

[a] Values are means ± SD (n = 3–10); δ_a and δ_b, limiting chemical shifts of the protonated and unprotonated form, respectively; $\Delta\delta_{ab} = \delta_a - \delta_b$.

All the new derivatives fulfilled both the desired conditions for more accurate pH probing (see Introduction), exhibiting near-neutral pK_as (ranging 6.28–6.97) and very high $\Delta\delta_{ab}$ values. Indeed, the average ^{31}P NMR sensitivities obtained here could compete with those of the best linear aminophosphonates available so far (Table S1). Interestingly, the compounds having no constrained phosphorus bound alkoxy groups such as **1a** and almost all elements from the crowded family showed slightly more basic pK_as and lower ^{31}P sensitivities when compared to compounds from the CyDEPMPHs family, for which $\Delta\delta_{ab}$ > 10 ppm. The only exception was compound **1f,** which retained a high sensitivity despite $\Delta\delta_{ab}$ = 9.35 ppm and a pK_a value in the range of that of the crowded DEPMPHs (Table 2).

In a biological milieu where NMR peaks are usually broad, any added pH probe should exhibit protonated and non-protonated forms in fast exchange on the NMR timescale to provide a single sharp peak for each cytosolic/intracellular compartment. This implies that the T_1 time of the probe should be as short as possible in order for the best resolved signals to be recorded within the timescale of expected variations of biological parameters, such as pH [28]. All new pH probes demonstrated T_1 values similar to those found in other related aminophosphonates [28,30]. Expectedly, molecular motion restriction in the conformationally constrained CyDEPMPHs **1b–f** versus the long-chain linear phosphonates **1l–p** from the crowded series generally resulted in slightly increased T_1 values (Table 2). It is worth noting that probe exchanges between cell compartments are slow on T_1 and chemical shift NMR timescales, while diffusion kinetics may exhibit strong variations for linear versus cyclic aminophosphonates (e.g., being 10 min for **1a** and 60 min for 2-aminoethylphosphonate (Figure 1B with R_1–R_3 = H and n = 2) [29]). Given that pH_i variations in vivo may occur in minutes (reported value were of ~10 min following acidosis [40] and 15–20 min following alkalinization [41]), T_1 does not therefore appear to be a decisive parameter to discriminate between probes having similar chemical structures.

2.3. pKa Modeling as a Function of Substituents

Predicting pK_a values by molecular modeling is of paramount importance in the design of improved ^{31}P NMR pH markers. In this regard, a pertinent approach is to consider the pH-dependent variations of electron density around the protonation site; that is, pK_a should depend linearly on the sum of individual inductive and stereochemical contributions of substituents. This has been applied successfully, first to a series of alkylphosphonic acids as depicted in Figure 1A [42], second to the cyclic and linear α-aminophosphonates developed in the early 2000s (see Figure 1C,D). In these studies [19,28], pK_as were computed using the semi-empirical linear model of Equation (1):

$$pK_a = a_0 + \sum a_i \times n_i \quad (1)$$

where, for a given structurally related family of compounds, a_0 is the pK_a of the common parent chemical structure and parameters n_i (with maximum $\Sigma n_i = 6$) and a_i (in pH units, with $1 < a_i < 10$) represent the number of each different kind of substituents of type i having the same structure and/or position relative to the nitrogen protonation site and the weight of its electronic effect relative to the pK_a value a_0, respectively.

Starting from the general dialkylamino structure with up to seven surrounding substituents, a new refinement, including compounds **1a–p**, of the previous a_i database collected from earlier studies afforded the updated Table S2 (see general structure in heading), where the selected reference structure bears a cycloalkyl substituent. The extended a_i database encompassed a total of 59 aminophosphonates, comprising **1a** and the new analogues **1b–p**, twenty-two linear (LAP-**1**–22) and ten cyclic (CAP-**1–10**)

aminophosphonates, five aminophosphophonic acid derivatives (APA-**1**–**5**), and six alkylamines (Tables S1 and S2) studied previously [19,22,28–31,39,43,44]. As shown in Figure 4, updating the a_i values still resulted in a good fit ($R^2 = 0.9876$) between experimental and calculated pK_as.

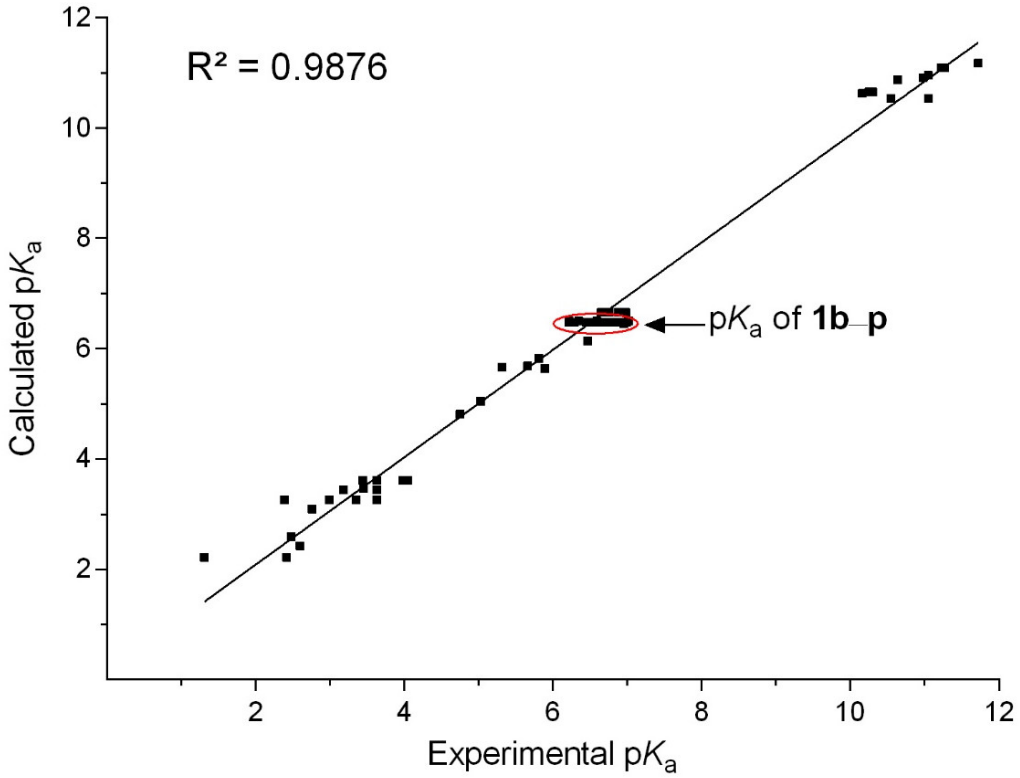

Figure 4. Correlation between experimental and calculated pK_a values for a pooled database of 59 α-aminophosphonates using the updated linear predictive model of Equation (1) (see also Table S2). The red circle indicates the pK_a domain of new compounds **1b**–**p**.

In the computational pK_as model of Equation (1), all compounds **1a**–**p** share the same substitution pattern, i.e., one H atom on the nitrogen, two C(5)–H, three alkyls on C(1) and C(5), and one C(1)–Phosphonate. Having the same {n_1–n_{10}} set of {1, 0, 2, 3, 0, 0, 0, 0, 1, 0}, compounds **1a**–**p** obviously yielded the same calculated pK_a = 6.475, while an experimental range of ΔpK_a = 0.75 was found (Table 2). When compared to this common pK_a value, the experimental pK_as of the more substituted compounds **1f** and **1i** were found to be strongly underestimated by 0.315 and 0.495 units, respectively (Table 2), suggesting that steric factors should be accounted for in the pK_as predictive model.

2.4. [C–P–O] Pyramidalization Angle Calculations

Previously, electrostatic interactions such as internal $^+NH_2\cdots$(O)P hydrogen bonding have been proposed to explain the shielding of the NMR peaks occurring upon protonation of α-aminophosphonates (i.e., $\delta_b > \delta_a$), an effect that would decrease the pyramidalization of the angle [C–P–O] of the tetrahedral phosphorylated moiety [19]. In view of the lack of accuracy of the predictive model of Equation (1) for the most sterically hindered new pH probes, it was investigated whether additional conformationally derived effects may be implicated.

DFT-B3LYP calculations using the Gaussian16 package were carried out for optimizing [C–P–O] angle variations between acidic and basic forms (Δ[C–P–O]$_{ab}$) for **1a**–**p**, pooled with the previously studied compounds LAP-**1**–**34**, CAP-**1**–**10**, and APA-**1**–**7** (Table S1) [19,22,28–32,39,43,45]. For this large set of compounds (corresponding to 78 pairs

of acidic and basic chemical shifts) a moderately good linear correlation ($y = 2.907\,x + 3.150$; $R^2 = 0.8816$) was obtained between $\Delta[C–P–O]_{ab}$ and $\Delta\delta_{ab}$ (Figure 5A), confirming that pyramidalization at phosphorus should have a notable impact on the ^{31}P NMR sensitivity of aminophosphonates. For simplification, the [C–P–O] pyramidalization angle α here was defined as the average of the three angles between P–O_{1-3} bonds and the *p*-plane orthogonal to the P–C bond (Figure 5B, inset); that is, α decreases as the pyramid is more flattened. Negative $\Delta[C–P–O]_{ab}$ variations associated to $\Delta\delta_{ab} < 0$ (i.e., $\delta_a > \delta_b$) were found for APA-**1**–**6** aminophosphonic derivatives (Table S1) in the pK_{a2} region of the second acidity (Figure 5A, region **I**, and Figure 5B, reactions I). A second group of molecules (Figure 5A, region **II**, and Figure 5B, reactions II) showed small changes in the pyramidalization angle ($0 < \Delta[C–P–O]_{ab} < 1.13°$), associated with low ^{31}P NMR sensitivities ($2.3 < \Delta\delta_{ab} < 5.3$ ppm). These latter structures bear at least two carbons between the N and P atoms of the phosphonic derivatives (LAP-**23**, APA-**2**,**5**–**7**; Table S1).

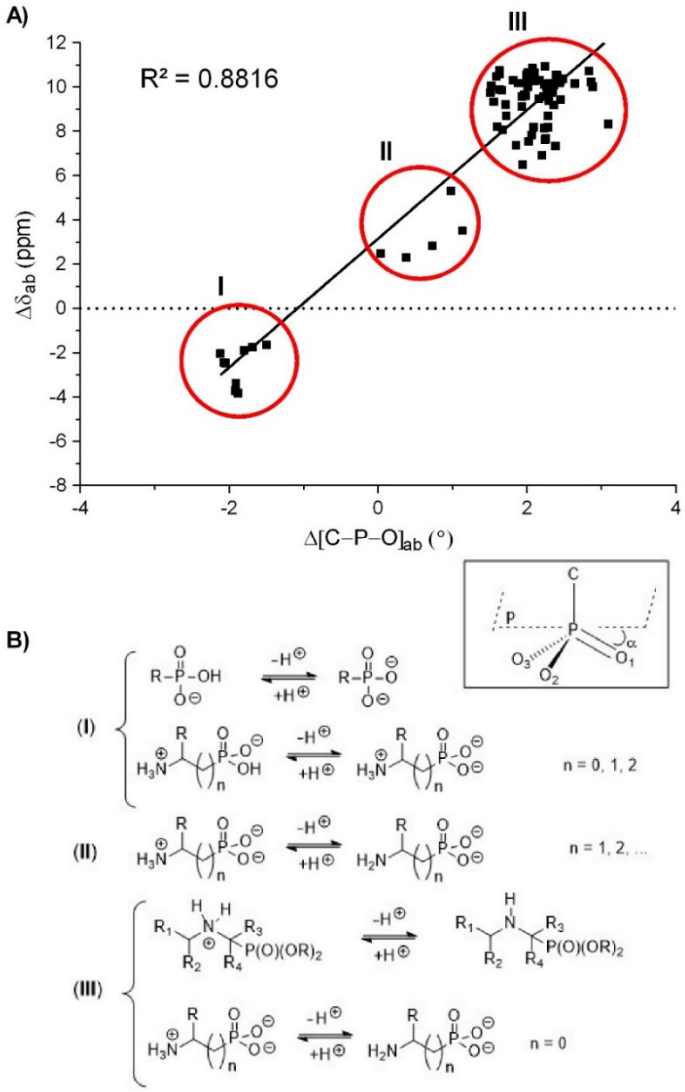

Figure 5. (**A**) Plot of ^{31}P NMR sensitivity against ab initio calculated pyramidalization angles at phosphorus between the acidic and basic forms of a series of phosphorylated pH probes. Circled regions I to III visualize increasing pH probing properties. (**B**) Proton exchange reactions on (I) the O atom of phosphonic or aminophosphonic acids, (II) the N atom of aminophosphonic compounds with at least two carbons between the N and P atoms and (III) the N atom of aminophosphonates or aminophosphonic acids with only one carbon between the N and P atoms. *Inset*: Pyramidalization angle α.

As anticipated behind the design of compounds **1b**–**p**, Figure 5A (region **III**) and Figure 5B (reactions III) show that those molecules having the largest Δ[C–P–O]$_{ab}$ (ranging 1.51–3.60°) also exhibited the greater $\Delta\delta_{ab}$s (6.48 < $\Delta\delta_{ab}$ < 10.94 ppm). Together with **1a**–**p**, region **III** compounds in Figure 5A also included the derivatives APA-**1**, LAP-**1**–**22**,**24**–**34**, and CAP-**1**–**10** (Table S1); that is, in all these molecules, the environment around P is moderately to strongly sterically crowded. Of interest, among the CyDEPMPHs, the apparently less constrained **1b** (Figure 2A), which bears a less bulky unsubstituted 1,3,2-dioxaphosphorinane ring, demonstrated the highest protonation-induced Δ[C–P–O]$_{ab}$ value of 2.10°.

2.5. In Vitro Cytotoxicity Studies

The cytotoxic activities of compounds **1a**–**p** in A549 human lung carcinoma cells and in normal human lung fibroblasts (NHLF) were evaluated in 0.2% DMSO-supplemented Dulbecco's modified Eagle's medium (DMEM) and fibroblast basal medium (FBM), respectively. The methods used included the tetrazolium dye MTT reduction, the fluorometric microculture cytotoxicity (FMCA), and the intracellular ATP assays. The MTT and FMCA assays are standard colorimetric determinations of cell viability during in vitro drug treatment while the ATP assay is an index of metabolic activity.

The IC_{50} values following 48 h incubation at 37 °C of the cells with varying concentrations of test compounds are reported in Table 3, together with the predicted lipophilicities based on AlogP calculations. When the three above-cited endpoints were found to be affected by treatment with a test compound, the release of cytosolic lactate dehydrogenase (LDH) was assessed to check for cell necrosis.

In the supernatant of untreated A549 and NHLF cells, the baseline LDH value was found to be 10.2 ± 1.5 and 11.3 ± 1.9 UI/mg protein, respectively. When compared to the total LDH activity measured after 100% lysis of the cells, which was 690 ± 47 and 701 ± 34 UI/mg protein for A549 and NHLF, respectively, the baseline released LDH vs. total cellular LDH in untreated cells was found to be as low as 1–2%.

After 48 h incubation of the cells, no significant dispersion among assays was found with compounds **1b**–**e** of the CyDEPMPHs family ($p > 0.05$ by one-way ANOVA), suggesting those aminophosphonates induced cell death by altering metabolic activity, enzymatic and mitochondrial functions rather than by causing membrane damage and/or cell necrosis. The more lipophilic **1d** and **1e** were found to be slightly more toxic (Table 3).

Regarding the three viability assays, the more lipophilic compound of the CyDEPMPHs family, **1f**, was associated with the strongest global decrease of IC_{50} values, which was of 42–50% ($p < 0.05$) as compared to **1b,** and reached 50–60% ($p < 0.05$) as compared to **1a**. In parallel, the application of **1f** resulted in a significant LDH leakage (>45% of total baseline LDH content; $p < 0.01$ vs. untreated cells and **1a, 1b**) showing it additionally caused cell necrosis.

Table 3. Cytotoxicity of α-Aminophosphonates Against A549 Cells and Normal Human Lung Fibroblasts (NHLF) [a], and their Calculated Lipophilicities.

Compounds	IC_{50} (mM) [b]						AlogP [c]
	FMCA		MTT		ATP		
	A549	NHLF	A549	NHLF	A549	NHLF	
1a	122 ± 8	112 ± 7	118 ± 11	110 ± 8	119 ± 7	109 ± 10	1.04
CyDEPMPHs family							
1b	95± 8	89 ± 5	92 ± 8	79 ± 6	85 ± 9	70 ± 7	0.26
trans-**1c**	80 ± 5	72 ± 7	76 ± 5	70 ± 3	69 ± 7	62 ± 6	0.54
cis-**1c**	77 ± 5	70 ± 5	78 ± 7	71 ± 9	67 ± 5	61 ± 5	0.54
1d	74 ± 9	69 ± 6	62 ± 5 *	58 ± 8 *	63 ± 5 *	56 ± 8	0.77
1e	70 ± 7 *	67 ± 8 *	65 ± 6 *	67 ± 7 *	62 ± 5 *	55 ± 5 *	1.51
1f	44 ± 6 *,†	35 ± 7 *,†	52 ± 9 *,†	45 ± 4 *,†	53 ± 4 *,†	47 ± 6 *,†	1.73
Crowded family							
1g	118 ± 9	104 ± 6	111 ± 3	97 ± 4	107 ± 9	92 ± 9	0.25
1h	101 ± 4	95 ± 7	97 ± 4	89 ± 2	98 ± 5	87 ± 5	1.65
1i	103 ± 3	98 ± 3	95 ± 4	90 ± 3	96 ± 4	89 ± 6	1.46
1j	18 ± 7 *,§	16 ± 7 *,§	30 ± 8 *,§	21 ± 7 *,§	31 ± 7 *,§	20 ± 8 *,§	2.31,§
1k	17 ± 6 *,§	14 ± 6 *,§	39 ± 5 *,§	29 ± 8 *,§	29 ± 7 *,§	14 ± 8 *,§	2.20,§
1l	11 ± 8 *,§	7 ± 6 *,§	21 ± 7 *,§	14 ± 5 *,§	23 ± 7 *,§	12 ± 8 *,§	3.31,§
1m	10 ± 4 *,§	8 ± 7 *,§	15 ± 4 *,§	11 ± 2 *,§	14 ± 3 *,§	13 ± 4 *,§	3.03,§
1n	12 ± 3 *,§	9 ± 4 *,§	16 ± 2 *,§	10 ± 2 *,§	17 ± 7 *,§	13 ± 6 *,§	2.92,§
1o	11 ± 5 *,§	7 ± 4 *,§	14 ± 3 *,§	11 ± 2 *,§	16 ± 3 *,§	12 ± 4 *,§	0.90,§
1p	13 ± 3 *,§	10 ± 4 *,§	16 ± 2 *,§	11 ± 2 *,§	20 ± 4 *,§	17 ± 4 *,§	0.25,§

[a] Cells seeded at 2.5×10^4 cells/well in DMEM (A549) or FBM (NHLF) until confluence were then incubated for 48 h at 37 °C with test compounds (0.01–100 mM) in culture medium + 0.2% DMSO (taken as vehicle). Data are means ± SD of 3–10 independent experiments made in triplicate for at least four concentrations. [b] IC_{50} defined as the concentration of compound resulting in 50% loss of cell viability after 48 h and calculated from concentration–response curves. [c] Calculated using the ALOGPS 2.1 software (available at Virtual Computational Chemistry Laboratory: www.vcclab.org/lab/alogps/ accessed on 25 July 2021). Statistics: one-way-ANOVA followed by the Newman–Keuls test: * $p < 0.05$ vs. **1b**, *trans*-**1c,** and *cis*-**1c**; † $p < 0.05$ vs. **1d** and **1e**; § $p < 0.05$ vs. **1g**, **1h**, and **1i.**

In the crowded family of pH probes, the decrease in viability globally paralleled the increase of lipophilicity, except for **1o** and **1p**. Hence, IC_{50} values for **1j**–**p** decreased by 60–80% ($p < 0.05$) as compared to the hydrophilic **1g** in the MTT and ATP assays, while an even greater impact was found for these lipophilic compounds in the FMCA assay (i.e., a 80–90% decrease; $p < 0.05$ vs. **1g**), suggesting they induced membrane damage at concentrations > 10 mM (Table 3). Consistently, application of **1j**–**p** to both types of cells resulted in a strong LDH leakage at IC_{50} values (60–80% of total baseline intracellular content).

Altogether, the cytotoxicity data of Table 3 demonstrated that most of the new pH probes, i.e., **1b**–**e** and **1g**–**i**, could be added safely in cell medium at a concentration window (up to 1–20 mM) compatible with NMR applications. Due to its innocuity and optimal ^{31}P NMR titration parameters ($pK_a = 6.45$; $\Delta\delta_{ab} = 10.64$ ppm), compound **1b** was considered ideal for probing small pH gradients, since it can be used at 4 mM, a concentration at which >98% cell viability was preserved.

2.6. Application of the ^{31}P NMR pH Probes **1b** *vs.* **1a** *in Dictyostelium discoideum Amoebae*

Dictyostelium discoideum, a widely used cell model for investigating acidic organelles, has been found to be particularly suitable to monitor by ^{31}P NMR the kinetics of anoxia- and reoxygenation-induced pH variations in various endosomal acidic vesicles [23]. In the search for improved resonance tools for assessing trans-sarcolemmal pH gradients, i.e., pH_i/pH_e differences, *D. discoideum* was also found to be a reliable model, since in this case endogenous and external ^{31}P NMR P_i peaks are easily distinguishable [21] and may allow a direct comparison with the expected resonances arising from the probe, provided it could significantly accumulate within the cytosolic and external compartments. Such properties were not reported in other models, including the rat heart [46] and liver [47] due, among other reasons, to the low and/or varying concentrations of P_i, the large line widths of cellular ^{31}P NMR peaks, and the low pH_i/pH_e difference <0.5 pH units.

Figure 6 shows representative ^{31}P NMR spectra obtained during incubation at 20 °C of normoxic amoebae in the presence of 4 mM of **1a** (lower trace, deshielded region) or **1b** (upper trace). In the more deshielded spectral region (20–30 ppm) of the experiment with **1b**, prominent resonances were apparent, likely arising from the probe internalized in cells and located in three distinct intracellular compartments. From the calibration curve of **1b** (Figure 3), the corresponding pH values were calculated as ~5.6 (for the more acidic compartment at 22.6 ppm) and 6.20 and 7.27 for the lowfield peaks at 25.4 and 29.9 ppm, respectively. These two latter compartments probed by **1b** likely correspond to the extracellular and cytosolic environments, in full accordance with the pH values determined by the two P_i peaks, pH_i ~7.24 (cytosol) and pH_e ~6.32 (extracellular milieu).

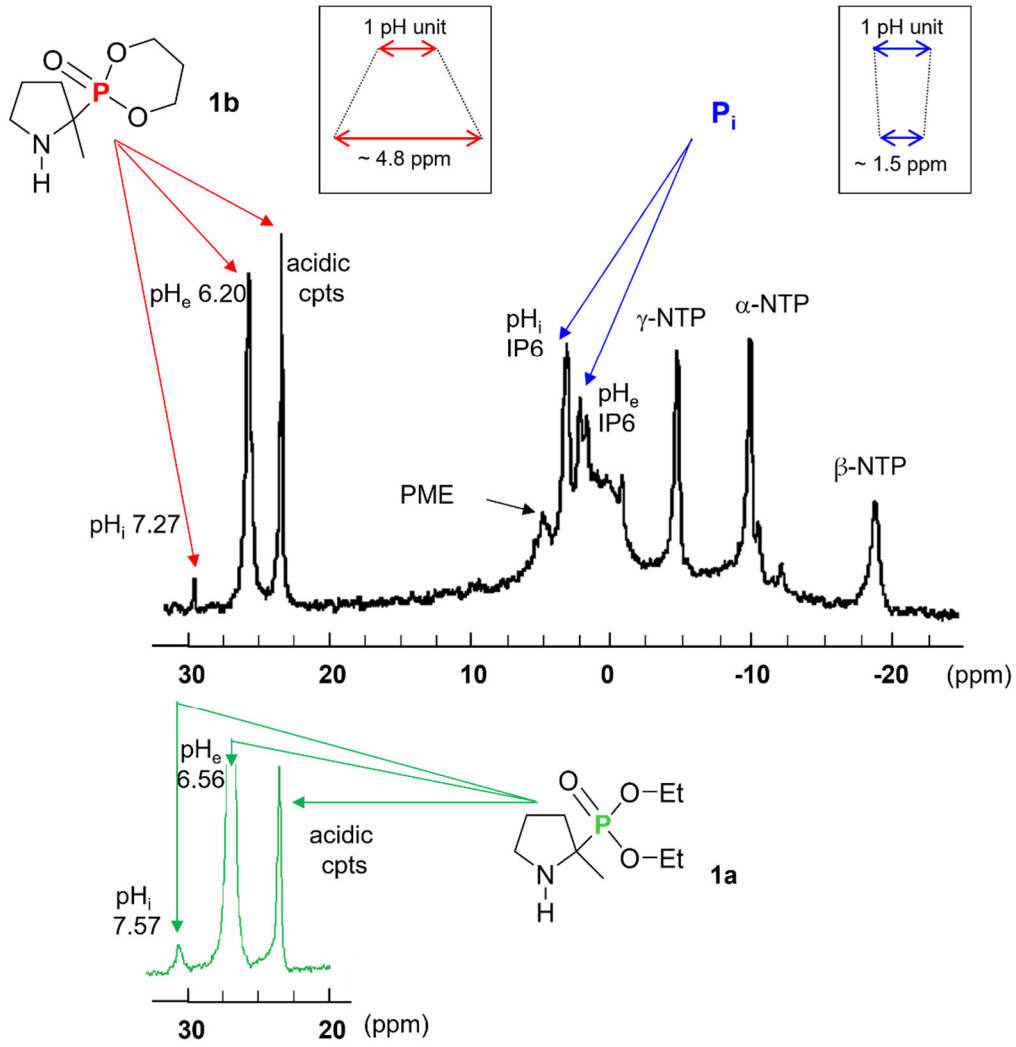

Figure 6. ^{31}P NMR spectra from *D. discoideum* cells (3 × 10^8 cells/mL) aerobically incubated at 20 °C in the presence of 4 mM of **1b** (upper trace) or **1a** (green trace, only deshielded region shown). The signals correspond to a 15-min accumulation (900 scans) starting 15 min after addition of the probe. Using the corresponding titration curves allowed for the simultaneous calculation of all pH values, i.e., intracellular (pH_i), extracellular (pH_e), and that of acidic compartments (cpts). Cytosolic and extracellular inorganic phosphate (P_i) pH values (pH_i ~7.24 and pH_e ~6.32) were drawn from the **1b** titration curve (Figure 3). Shielded resonances in the upper trace are from phosphomonoesters (PME); inositol hexaphosphate (IP6); γ-, α-, and β-nucleoside triphosphates (NTPs) [21,29]. Chemical shifts are given in ppm with respect to 85% external H_3PO_4 at 0 ppm and to 50 mM methylene diphosphonate (pH 8.9) placed in a capillary and used as an additional standard at 16.4 ppm. *Insets*: a schematic representation for comparison between **1b** and P_i pH probing accuracies around their pK_a values.

When **1a** was used instead of **1b,** acidic compartments were similarly probed at 23.6 ppm (pH~5.7) while the cytosolic and extracellular regions exhibited broader lines and higher apparent pH values of pH_i 7.57 (resonance at 30.5 ppm) and pH_e ~6.56 (broad resonance at ~26.5 ppm), respectively. This showed that **1a** accumulated mainly in the external space vs. the cytosol and confirmed the previous observations [29] of (i) a line broadening at the resonance corresponding to the cytosolic pH, and (ii) a slight alkalinization of the cytosolic and extracellular compartments because of the higher pK_a of the probe, which behaved as a weak base.

The innocuity of **1b** (4 mM) in the system was confirmed by its lack of effect on the endogenous intracellular phosphorylated compounds including nucleotides, inositol hexakisphosphate and phosphomonoesters, as compared to control spectra (data not shown). As already reported with other series of cyclic and linear α-aminophosphonates [29], **1b** was internalized in amoebae in less than 5 min (data not shown) both in the cytosol, extracellular region and acidic vesicles. To explain the rapid rate of diffusion and intracellular distribution observed for **1b** and other aminophosphonates [27,29], it was supposed that these compounds are membrane permeable under their unprotonated amine form, and can accumulate by passive diffusion [29]. This general property confers a great advantage to α-aminophosphonates as compared to the commonly used alkylated phosphonic acids derivatives, which were shown to internalize slowly, at least during 90 min, within the cells, involving energy requiring processes such as continuous H^+ pumping by vacuolar H^+–ATPase, leading to NTP depletion [48].

To stress on the specific ^{31}P NMR pH reporting properties, the biocompatible **1b** showed a ~3.2 better potential accuracy than P_i (Figure 6). This may allow us to reliably address pH differences as low as 0.05 pH units, corresponding to narrow peaks separated by ~0.25 ppm. As anticipated in the design of the novel pH probes, this property results from their improved $\Delta\delta_{ab}$ values, giving a steepest slope around pK_as close to that of P_i.

3. Materials and Methods

3.1. Chemistry

All reagents and solvents were of the highest grade available from Sigma-Aldrich, Fluka, SDS, or Acros, and were used without further purification, except for 2-methyl-1-pyrroline (from Acros Organics, Halluin, France), which was distilled under reduced pressure (20 mm Hg, bp: 50 °C) before use. Diethyl H-phosphonate (**2a**), dimethyl H-phosphonate (**2g**), di(isopropyl) H-phosphonate (**2i**), and di-*n*-butyl H-phosphonate (**2j**) were from Acros. The dialkyl H-phosphonates **2b–f** and the aminophosphonates **1b–f** belonging to the CyDEPMPHs family were synthesized and purified as previously described [39]. DEPMPH (**1a**) [19], and its analogue **1i** [49], and dialkyl H-phosphonates **2h** and **2n**, and aminophosphonates **1g**, **1h**, and **1n** [29] were synthesized and purified as previously described. Reactions were followed by thin layer chromatography (TLC) on Merck-Kieselgel 60 F254 precoated silica gel plates, and the spots were visualized by staining with phosphomolybdic acid. NMR spectra (^1H NMR at 300 MHz, ^{13}C NMR at 75.5 MHz and ^{31}P NMR at 121.5 MHz) were recorded on a Bruker AVL 300 spectrometer. Chemical shifts (δ) are expressed in ppm (parts per million) relative to internal tetramethylsilane (^1H and ^{13}C) or external 85% H_3PO_4 (^{31}P), and coupling constants *J* are given in Hz. The abbreviations s, d, t, m and q refer to singlet, doublet, triplet, multiplet and quartet signals, respectively. Melting points were determined using a B-540 Buchi apparatus and are uncorrected. Elemental analyses were performed using a Thermo Finnigan EA-1112 analyzer and were within 0.2% of theoretical values. Column chromatography was performed on Merck silica gel 60 (230~400 mesh).

3.1.1. Synthesis of Dialkyl H-Phosphonates **2k–m**, **2o**, and **2p**

Water (1.1 g, 61 mmol) was added to HMPT (10 g, 61 mmol) in refluxing anhydrous THF (20 mL) under argon atmosphere and the mixture was stirred at reflux for 2 h. Then the corresponding alcohol (122 mmol) was added and the mixture was refluxed for another 2 h. Afterwards, the mixture was concentrated under reduced pressure to give the corresponding dialkyl H-phosphonate **2k–m, 2o**, and **2p** in high yields (95–98%) and a purity of >95% determined by ^{31}P NMR. ^{31}P NMR (121.5 MHz, $CDCl_3$) δ **2k**, 8.42; **2l**, 8.05; **2m**, 7.80; **2o**, 9.39; **2p**, 9.53.

3.1.2. General Procedure for Synthesis of Compounds **1j**–**m**, **1o**, and **1p**

A mixture of 2-methyl-1-pyrroline (1.1 eq) and the corresponding dialkyl H-phosphonate (1 eq) was stirred at room temperature until completion. TLC or ^{31}P NMR were used to follow the reaction. The mixture was poured into water (aminophosphonate final concentration, ~1.8 M) and slowly acidified to pH 3 with concentrated HCl. The aqueous layer was extracted with TBME (3 × volume of water), basified with NaOH pellets to pH 9–10, and extracted with CH_2Cl_2 (4 × volumes of water). The combined organic phases were dried over $MgSO_4$, filtered and concentrated under reduced pressure. The residue was purified by SiO_2 column chromatography with a CH_2Cl_2:EtOH mixture as eluent to yield the expected aminophosphonates.

Di-n-butyl (2-methylpyrrolidin-2-yl)phosphonate (**1j**). Title compound was obtained by stirring 2-methyl-1-pyrroline (10 g, 120 mmol) with commercially available di-*n*-butyl H-phosphonate (21.1 g, 109 mmol) for 10 days. Flash chromatography using a CH_2Cl_2:EtOH, 90:10, v:v as eluent yielded **1j** as a yellow oil (22.3 g, 67%); ^{1}H NMR (300 MHz, $CDCl_3$) δ 4.06–3,97 (m, 4H, 2 × O-CH_2), 3.04–2.88 (m, 2H, 5-CH_2), 2.22–2.10 (m, 1H, 3-C(H)H), 1.83–1.70 (m, 4H, NH, 3-C(H)H, 4-CH_2), 1.64–1.51 (m, 5H, 2 × O-CH_2-CH_2 and 3-C(H)H), 1.37–1.28 (q, *J* = 6.0 Hz, 4H, 2 × CH_2-CH_3), 1.27 (d, *J* = 15.0 Hz, 3H, 2-C(CH_3)), 0.87 (t, *J* = 6.0 Hz, 6H, O-(CH_2)$_3$-CH_3); ^{13}C NMR (75.5 MHz, $CDCl_3$) δ 66.0 (d, *J* = 8.2 Hz, O-CH_2), 65.8 (d, *J* = 8.2 Hz, O-CH_2), 59.2 (d, *J* = 163.8 Hz, 2-C), 47.0 (d, *J* = 7.5 Hz, 5-C), 34.3 (d, *J* = 3.0 Hz, 3-C), 32.7 (d, *J* = 2.5 Hz, O-CH_2-CH_2), 32.6 (d, *J* = 2.5 Hz, O-CH_2-CH_2), 25.6 (d, *J* = 4.5 Hz, 4-C), 24.2 (d, *J* = 6.0 Hz, 2-C(CH_3)), 18.7 (2C, CH_2-CH_3), 13.5 (2 × O-(CH_2)$_2$-CH_3); ^{31}P NMR (121.5 MHz, $CDCl_3$) δ 31.03. Elemental analysis calcd (%) for $C_{13}H_{28}NO_3P$: C 56.30, H 10.18, N 5.05; found: C 54.72, H 10.10, N 5.01.

Diisobutyl (2-methylpyrrolidin-2-yl)phosphonate (**1k**). Title compound was obtained by stirring 2-methyl-1-pyrroline (5.5 g, 66 mmol) with commercially available diisobutyl H-phosphonate **2k** (11.8 g, 60 mmol) for 7 days. Flash chromatography using a CH_2Cl_2:EtOH, 90:10, v:v as eluent yielded **1k** as a yellow oil (11.8 g, 70%); ^{1}H NMR (300 MHz, $CDCl_3$) δ 3.54–3.43 (m, 4H, 2 × O-CH_2), 2.73–2.57 (m, 2H, 5-CH_2), 1.95–1.88 (m, 1H, 3-C(H)H), 1.63–1.24 (m, 6H, NH, 3-C(H)H, 4-CH_2, 2 × $CH(CH_3)_2$), 0.98 (d, *J* = 15.0 Hz, 3H, 2-C(CH_3)), 0.60–0.57 (d, *J* = 6.0 Hz, 12H, 2 × $CH(CH_3)_2$); ^{13}C NMR (75.5 MHz, $CDCl_3$) δ 71.4 (d, *J* = 7.5 Hz, O-CH_2), 71.1 (d, *J* = 7.5 Hz, O-CH_2), 58.8 (d, *J* = 165.3 Hz , 2-C), 46.2 (d, *J* = 7.5 Hz, 5-C), 32.9 (d, *J* = 2.5 Hz, 3-C), 28.4 (2 × $CH(CH_3)_2$), 24.5 (d, *J* = 4.5 Hz, 4-C), 23.5 (d, *J* = 6.0 Hz, 2-C(CH_3)), 17.8 (2 × $CH(CH_3)_2$); ^{31}P NMR (121.5 MHz, $CDCl_3$) δ 31.17. Elemental analysis calcd (%) for $C_{13}H_{28}NO_3P$: C 56.30, H 10.18, N 5.05; found: C 55.06, H 10.56, N 4.96.

Dipentyl (2-methylpyrrolidin-2-yl)phosphonate (**1l**). Title compound was obtained by stirring 2-methyl-1-pyrroline (2.5 g, 30 mmol) with dipentyl H-phosphonate **2l** (6 g, 27.3 mmol) for 7 days. Flash chromatography using a CH_2Cl_2:EtOH, 90:10, v:v as eluent yielded **1l** as a yellow oil (4.2 g, 49%); ^{1}H NMR (300 MHz, $CDCl_3$) δ 4.07–3.99 (m, 4H, 2 × O-CH_2), 3.07–2.91 (m, 2H, 5-CH_2), 2.22–2.18 (m, 1H, 3-C(H)H), 1.90–1.52 (m, 8H, 2 × OCH_2CH_2, NH, 3-C(H)H, 4-CH_2), 1.30 (m, 8H, 2 × $CH_2CH_2CH_3$), 1.30 (d, *J* = 15.0 Hz, 3H, 2-C(CH_3)), 0.86 (t, *J* = 9.0 Hz, 6H, 2 × CH_2CH_3); ^{13}C NMR (75.5 MHz, $CDCl_3$) δ 66.4 (d, *J* = 7.5 Hz, O-CH_2), 66.1 (d, *J* = 7.5 Hz, O-CH_2), 59.6 (d, *J* = 164.6 Hz, 2-C), 47.1 (d, *J* = 7.5 Hz, 5-C), 34.6 (d, *J* = 2.5 Hz, 3-C), 30.4 (d, *J* = 4.5 Hz, 4-C), 27.6 (2C, $CH_2CH_2CH_3$), 25.7 (d, *J* = 4.5 Hz, 2C, OCH_2CH_2), 24.3 (d, *J* = 6.8 Hz , 2-C(CH_3)), 22.2 (2 × CH_2CH_3), 13.9 (2C, CH_2CH_3); ^{31}P NMR (121.5 MHz, $CDCl_3$) δ 30.95. Elemental analysis calcd (%) for $C_{15}H_{32}NO_3P$: C 58.99, H 10.56, N 4.59; found: C 56.10, H 10.35, N 3.90.

Diisopentyl (2-methylpyrrolidin-2-yl)phosphonate (**1m**). Title compound was obtained by stirring 2-methyl-1-pyrroline (4.4 g, 53 mmol) with diisopentyl H-phosphonate **2m** (10.8 g, 48.2 mmol) for 7 days. Flash chromatography using a CH_2Cl_2:EtOH, 90:10, v:v as eluent yielded **1m** as a yellow oil (4.2 g, 49%); ^{1}H NMR (300 MHz, $CDCl_3$) δ 4.07–3.99 (m, 4H, 2 ×O-CH_2), 3.07–2.91 (m, 2H, 5-CH_2), 2.22–2.18 (m, 1H, 3-C(*H*)H), 1.90–1.52 (m, 8H, 2 × OCH_2CH_2, NH, 3-C(*H*)H, 4-CH_2), 1.30 (m, 8H, 2 × $CH_2CH_2CH_3$), 1.30 (d, *J* = 15.0 Hz, 3H, 2-C(CH_3)), 0.86 (t, *J* = 9.0 Hz, 6H, 2 × CH_2CH_3); ^{13}C NMR (75.5 MHz, $CDCl_3$) δ 66.4 (d, *J* = 7.5 Hz, O-CH_2), 66.1 (d, *J* = 7.5 Hz, O-CH_2), 59.6 (d, *J* = 164.6 Hz, 2-C), 47.1 (d, *J* = 7.5 Hz, 5-C), 34.6 (d, *J* = 2.5 Hz, 3-C), 30.4 (d, *J* = 4.5 Hz, 4-C), 27.6 (2C, $CH_2CH_2CH_3$), 25.7 (d, *J* = 4.5 Hz, 2C, OCH_2CH_2), 24.3 (d, *J* = 6.8 Hz , 2-C(CH_3)), 22.2 (2 × CH_2CH_3), 13.9 (2C, CH_2CH_3); ^{31}P NMR (121.5 MHz, $CDCl_3$) δ 30.95. Elemental analysis calcd (%) for $C_{15}H_{32}NO_3P$: C 58.99, H 10.56, N 4.59; found: C 56.10, H 10.35, N 3.90.

Di(2-ethoxyethyl)(2-methylpyrrolidin-2-yl)phosphonate (**1o**). Title compound was obtained by stirring 2-methyl-1-pyrroline (2.5 g, 30 mmol) with diethoxyethyl H-phosphonate **2o** (6.2 g, 27.3 mmol) for 1 day. Flash chromatography using a CH_2Cl_2:EtOH, 96:4, v:v as eluent yielded **1o** as a yellow oil (6.1 g, 73%); ^{1}H NMR (300 MHz, $CDCl_3$) δ 4.23–4.11 (m, 4H, 2 × P-O-CH_2), 3.66–3.62 (t, *J* = 6.0 Hz, 4H, 2 × $CH_2OCH_2CH_3$), 3.57–3.50 (q, *J* = 6.0 Hz, 4H, 2 × CH_2CH_3), 3.02–2.90 (m, 2H, 5-CH_2), 2.25–2.17 (m, 1H, 3-C(*H*)H), 1.90–1.53 (m, 4H, 3-C(*H*)H, 4-CH_2, NH), 1.31 (d, *J* = 15.0 Hz, 2-C(CH_3)), 1.13 (t, *J* = 9.0 Hz, 6H, 2 × CH_2CH_3); ^{13}C NMR (75.5 MHz, $CDCl_3$) δ 69.7 (d, *J* = 5.3 Hz, 2 × $CH_2OCH_2CH_3$), 66.5 (2 × CH_2CH_3), 65.2 (d, *J* = 7.5 Hz, P-O-CH_2), 65.3 (d, *J* = 7.5 Hz, P-O-CH_2), 59.7 (d, *J* = 163.8 Hz, 2-C), 46.9 (d, *J* = 6.8 Hz, 5-C), 34.6 (d, *J* = 3.8 Hz, 3-C), 25.6 (d, *J* = 3.8 Hz, 4-C), 24.2 (d, *J* = 6.8 Hz, 2-C(CH_3)), 15.1 (2C, CH_2CH_3); ^{31}P NMR (121.5 MHz, $CDCl_3$) δ 31.65. Elemental analysis calcd (%) for $C_{13}H_{28}NO_3P$: C 50.48, H 9.12, N 4.53; found: C 49.16, H 9.03, N 4.39.

Di(2,5,8,11-tetraoxatridecan-13-yl)(2-methylpyrrolidin-2-yl)phosphonate (**1p**). Title compound was obtained by stirring 2-methyl-1-pyrroline (0.6 g, 7.5 mmol) with di(2,5,8,11-tetraoxatridecan-13-yl) H-phosphonate **2p** (3.2 g, 6.8 mmol) for 1 day. Flash chromatography using a CH_2Cl_2:EtOH, 96:4, v:v as eluent yielded **1q** as a yellow oil (2.7 g, 71%); ^{1}H NMR (300 MHz, $CDCl_3$) δ 4.30–4.12 (m, 4H, 2 × $POCH_2$), 3.71–3.65 (m, 4H, 2 × OCH_2), 3.65–3.58 (m, 20H, 10 × OCH_2), 3.55–3.49 (m, 4H, 2 × OCH_2), 3.33 (6H, 2 × OCH_3), 3.10–2.91 (m, 2H, 5-CH_2), 2.28-–2.17 (m, 1H, 3-C(*H*)H), 1.90–1.52 (m, 4H, 3-C(*H*)H, 4-H, NH), 1.32 (d, *J* = 15.0 Hz, 2-C(CH_3)); ^{13}C NMR (75.5 MHz, $CDCl_3$) δ 72.7 (OCH_2), 71.8 (OCH_2), 70.5 (OCH_2), 70.4 (OCH_2), 70.3 (OCH_2), 70.1 (OCH_2), 65.3 (d, *J* = 7.5 Hz, $POCH_2$), 65.2 (d, *J* = 7.5 Hz, $POCH_2$), 59.7 (d, *J* = 164.6 Hz, 2-C), 58.9 (2C, OCH_3), 46.9 (d, *J* = 7.5 Hz, 5-C), 34.5 (d, *J* = 2.3 Hz 3-C), 25.5 (d, *J* = 4.5 Hz, 4-C), 23.0 (d, *J* = 6.8 Hz, 2-C(CH_3)); ^{31}P NMR (121.5 MHz, $CDCl_3$) δ 29.52. Elemental analysis calcd (%) for $C_{23}H_{48}NO_{11}P$: C 50.63, H 8.87, N 2.57; found: C 47.67, H 8.84, N 2.37.

3.2. X-ray Crystallography

CyDEPMPHs were dissolved in the minimum of CH_2Cl_2, recrystallized from TBME, and dried in a vacuum to give single crystals suitable for X-ray diffraction studies. Intensities were collected at 293 K on a Nonius Kappa CCD diffractometer (Bruker) using graphite-monochromated $Mo_{K\alpha}$ radiation (λ = 0.71073 Å).

Crystal data for **1b**: $C_8H_{16}NO_3P$ *M* = 205.20, monoclinic space group *P*-21 c, Hall group *-P 2ybc*, *a* = 12.3308(2), *b* = 13.7792(2), *c* = 15.2243(2) Å, *β* = 126.3761(7)°, *V* = 2082.69(5) Å^3, *Z* = 4.

Crystal data for *trans*-**1c**: $C_9H_{18}NO_3P$ M = 219.21, monoclinic space group P-21 c, Hall group *-P 2ybc*, a = 6.6716(1), b = 12.6291(2), c = 13.6892(3) Å, β = 92.9872(8)°, V = 1151.83(4) Å^3, Z = 4.

Crystal data for **1d**: $C_{10}H_{20}NO_3P$ M = 233.24, monoclinic space group P-21 c, Hall group *-P 2ybc*, a = 10.5502(5), b = 11.1665(4), c = 11.4207(2) Å, V = 1214.42(9) Å^3, Z = 4.

Crystal data for **1e**: $C_{12}H_{24}NO_3P$ M = 261.29, orthorhombic space group Pbca, Hall group *-P 2ac 2ab*, a = 13.3114(2), b = 10.4734(2), c = 20.0050(2) Å, V = 2789.01(9) Å^3, Z = 8.

Crystal data for **1f**: $C_{12}H_{24}NO_3P$ M = 261.29, triclinic space group P-1, Hall group *-P 1*, a = 6.5802(5), b = 7.9200(9), c = 14.228(1) Å, V = 699.37(11) Å^3, Z = 2.

CCDC 794184, 794158, 794208, 794102, 793,993 contains the supplementary crystallographic data of **1b**, *trans*-**1c**, **1d–f**, respectively. These data are provided free of charge by The Cambridge Crystallographic Data Centre, 12 Union Road, Cambridge, UK (fax: +44 1223 336033; e-mail: deposit@ccdc.cam.ac.uk).

3.3. P NMR pH-Titration of Aminophosphonates 1a-p

All titrations were carried out at 22 °C in modified KH medium (pH 7.35), consisting of (in mM): KH_2PO_4, 1.2; $MgSO_4$, 1.2; NaCl, 118.5; KCl, 4.8; $NaHCO_3$, 25, and EDTA, 0.55 dissolved in doubly distilled deionized water. Spectra were acquired (32 scans) at 22 °C on a Bruker AMX 400 spectrometer with a 9.4 Tesla wide-bore magnet at a phosphorus frequency of 161.98 MHz. Samples were placed in 10-mm tubes. ^2H_2O in a small capillary was used as a lock signal for the spectrometer. Chemical shifts are given in ppm with respect to 85% external H_3PO_4 at 0 ppm and were plotted against pH to fit the Henderson–Hasselbach Equation (2) for NMR using nonlinear regression (Prism, GraphPad Software Inc., San-Diego, CA, USA):

$$pH = pK_a + \log\left[\frac{\delta - \delta_a}{\delta_b - \delta}\right] \quad (2)$$

where δ is the experimental ^{31}P chemical shift and the δ_a and δ_b correspond to the limiting chemical shift values of protonated and unprotonated amines forms, respectively. Calculated titration data (pK_a, δ_a, δ_b and their difference ($\Delta\delta_{ab}$)) are expressed as mean ± SD.

3.4. Computational Methods for [C–P–O] Angle Calculations

[C–P–O] angle calculations were performed for both acidic and basic forms of the aminophosphonates. To improve the accuracy of the calculations for compounds **1a–p**, compounds LAP-**1–34**, CAP-**1–10**, APA-**1–5** (Table S1), and 6 amines (i.e., dimethylamine, diethylamine, diisopropylamine, piperidine, pyrrolidine, tetramethylpiperidine) were included to the pooled molecules. The angle calculations were performed using Gaussian16 software [50] after geometry optimization at B3LYP/6-31G(d) level of theory. To obtain the most stable conformation of each molecule before DFT optimization, a simulated annealing calculation at the AM1 level with the Ampac 11 [51] software package was performed. The optimizations were achieved with a maximum time of 12 h. A check for the absence of imaginary frequencies and a gradient close to zero was performed. All calculations were performed in water solvent with the Polarizable Continuum Model (PCM) [52]. Data (in °) are expressed as the differences in [C–P–O] angles between the acidic and basic structures (Δ[C–P–O]$_{ab}$).

3.5. Cell Culture, Cytotoxicity Assays, and pH Assessment in Amoebae

DMEM, GlutaMax™, and phosphate-buffered saline (PBS) were obtained from Gibco Life Technologies Inc. (Thermo Fisher Scientific, Illkirch, France). FBM and growth factors (FGM; Clonetics FGM-2 Bullet Kit) were from Lonza (Amboise, France). A549 (ATCC CCL-185; LGC Standards, Molsheim, France) and NHLF (Lonza) cells were routinely maintained in [DMEM + GlutaMax] and [FBM + FGM], respectively, as described previously [53,54]. After reaching 90% confluence, cells were harvested for subculture. Cells were trypsinized, seeded in 96-well microplates (density, 2.5×10^4 cells/well) and incubated at 37 °C in a humidified atmosphere with 5% CO_2 to reach ~80% confluence in the appropriate medium. The medium was renewed and cells were exposed for 48 h to the tested compounds (1–1000 μg/mL) or DMSO (0.2%) added medium (control). Afterwards, cells were washed twice with PBS 1X (+/+) for cytotoxicity analysis. Supernatant medium samples were kept to evaluate cytosolic LDH release using a commercial kit (Biolabo, Maisy, France). To estimate the total LDH content, a control measurement was performed for each set of experiments by treating cells with 1% Triton X-100 to induce a total LDH release in the supernatant and induce a 100% loss of viability.

The FMCA and MTT assays were carried out as described [55]. Intracellular ATP content was assayed using a luciferin–luciferase reagent (Biofax A®; Yelen Analytics, Marseille, France; http://www.yelen-analytics.com (accessed on 10 January 2021)) according to [55]. IC_{50} values, defined as the concentration of test compounds resulting in 50% cell viability after 48 h, were calculated from concentration–response curves (PrismSoftware) and are expressed as mean ± SD (standard deviation relative to the mean from 3–10 independent experiments).

3.6. Dictyostelium Discoideum Cells Cultures and ^{31}P NMR

D. discoideum amoebae, axenic strain (ATCC 24397), were cultured aerobically as previously described [21,29]. Briefly, cells were harvested in their exponential growth phase, washed with ice-cold 20 mM 2-morpholinoethanesulfonic acid sodium salt (MES-Na) buffer and then suspended (3×10^8 cells/mL) at 20 °C under O_2 bubbling in MES-Na (20 mM), 6% ^2H_2O and 5 μL of Antifoam 289 (Sigma-Aldrich, Saint Quentin Fallavier, France) to a final volume of 20 mL (pH 6.5). Afterwards, **1a** or **1b** were added (4 mM final concentration) to the cell medium and incubation was prolonged for up to 30 min at 20 °C.

Incubation samples were then placed in 25-mm NMR tubes and an ^2H_2O sample, placed in a small capillary, was used as a lock signal for the NMR spectrometer. ^{31}P NMR spectra were routinely recorded during cell incubation at 20 °C on a Bruker AMX 400 spectrometer with a 9.4 T wide-bore magnet at a phosphorus frequency of 161.98 MHz. Chemical shifts are given in ppm with respect to 85% external H_3PO_4 at 0 ppm and to 50 mM methylene diphosphonate (pH 8.9), placed in a capillary and used as an additional standard at 16.4 ppm. Spectral acquisitions were carried out using a 60° (10 μs) pulse width, a 0.28 s acquisition time, a 0.72 s repetition delay, and gated Waltz proton decoupling [21]. Data were stored during 120 min as 300-scan (5 min) or 900-scan (15 min) blocks. Gaussian line broadening (GB = 0.05, LB = –5 Hz) was applied prior to Fourier transformation. The extracellular and intracellular distribution of the probe was determined by the respective areas of the corresponding resonances.

3.7. Statistics

Titration and biological values are expressed as mean ± SD. Differences were analyzed using a one-way analysis of variance (ANOVA) followed by *a posteriori* Newman–Keuls test. Intergroup differences were considered to be significant at $p < 0.05$.

4. Conclusions

A novel series of fifteen α-aminophosphonates have been synthesized and screened for their ^{31}P NMR properties in the probing of subtle pH changes (as low as 0.05 pH units) occurring in normal or acidotic cells. The new compounds, obtained in only two or three synthetic steps, showed the following enhanced properties: (i) chemical shifts in the 18–36 ppm range distinct from those of phosphorus metabolites; (ii) near-neutral pK_as (6.3–7.0); (iii) a high NMR sensitivity ($\Delta\delta_{ab}$ ranging 9.2–10.6 ppm) that can be modulated by adjusting the substituents and steric effects around the phosphorus atom; (iv) no cytotoxic effect for most of them in the concentration range used for biological NMR applications (up to 20 mM); (v) the ability to penetrate the compartments of interest (i.e., intra- and extracellular media); (vi) protonated and non-protonated forms in fast exchange on the NMR timescale, thus providing a single signal for each compartment. The hit compound **1b** was applied successfully to accurately measure a trans-sarcolemmal pH gradient in *D. discoideum*. It is believed this aminophosphonate may be widely used to study the proton exchange dynamics between cellular compartments.

Supplementary Materials: The following are available online at www.mdpi.com/article/10.3390/molecules27144506/s1, Table S1: pK_a and $\Delta\delta_{ab}$ values in KH medium reported in the literature for various aminophosphosphorylated compounds; Table S2: Substituents types and Increments a_i for pK_a calculation using Equation (1).

Author Contributions: Conceptualization, S.P.; methodology, E.R., B.B., D.S. and S.P.; validation, M.C. (Marcel Culcasi), S.P. and S.T.-L.; formal analysis, M.C. (Marcel Culcasi), S.P. and S.T.-L.; investigation, C.D., E.R., M.C. (Mathieu Cassien) and B.B.; data curation, D.S., B.B, M.C. (Marcel Culcasi), E.R., M.C. (Mathieu Cassien), S.P. and S.T.-L.; writing—original draft preparation, C.D. and E.R.; writing—review and editing, M.C. (Marcel Culcasi), S.P. and S.T.-L.; supervision, M.C. (Marcel Culcasi), S.P. and S.T.-L.; project administration, S.P.; funding acquisition, M.C. (Marcel Culcasi), S.P. and S.T.-L. All authors have read and agreed to the published version of the manuscript.

Funding: This work was funded by the MNERT (CNRS-UMR 7273, Institut de Chimie Radicalaire) grants program to C.D. Authors thank Yelen Analytics (Marseille, France) for financial support in cell culture studies. Part of this study (chemistry, NMR titrations, biological NMR) was supported by fundings of the Agence Nationale de la Recherche, France (ANR ROS Signal—N° ANR-09-BLAN-005-03). Other part of this study (pK_a modeling and CPO angle calculations) was supported by fundings of the Agence Nationale de la Recherche, France (ANR JCJC MitoDiaPM—N° ANR-17-CE34-0006-01).

Institutional Review Board Statement: Not applicable.

Informed Consent Statement: Not applicable.

Data Availability Statement: The data presented in this study are available on request from the authors.

Acknowledgments: Authors thank G. Gosset for her very valuable contribution to synthesis and titration experiments, M. Giorgi for his kind help in collection of crystallographic data and Prof. M. Satre (UMR 5092 CNRS CEA and University Joseph Fournier, Grenoble, France) for expert assistance in NMR experiments on *Dictyostelium discoideum* amoebae.

Conflicts of Interest: The authors declare no conflict of interest.

Sample Availability: Samples of the compounds are not available from the authors.

References

1. Casey, J.R.; Grinstein, S.; Orlowski, J. Sensors and regulators of intracellular pH. *Nat. Rev. Mol. Cell Biol.* **2010**, *11*, 50–61. https://doi.org/10.1038/nrm2820.
2. Moon, R.B.; Richards, J.H. Determination of intracellular pH by ^{31}P magnetic resonance. *J. Biol. Chem.* **1973**, *248*, 7276–7278. https://doi.org/10.1016/S0021-9258(19)43389-9.
3. Cohen, S.M.; Ogawa, S.; Rottenberg, H.; Glynn, P.; Yamane, T.; Brown, T.R.; Shulman, R.G. ^{31}P nuclear magnetic resonance studies of isolated rat liver cells. *Nature* **1978**, *273*, 554–556. https://doi.org/10.1038/273554a0.
4. Barton, J.K.; den Hollander, J.A.; Lee, T.M.; MacLaughlin, A.; Shulman, R.G. Measurement of the internal pH of yeast spores by ^{31}P nuclear magnetic resonance. *Proc. Natl. Acad. Sci. USA* **1980**, *77*, 2470–2473. https://doi.org/10.1073%2Fpnas.77.5.2470.
5. Adam, W.R.; Koretsky, A.P.; Weiner, M.W. 31P-NMR in vivo measurement of renal intracellular pH: Effects of acidosis and K^+ depletion in rats. *Am. J. Physiol*. **1986**, *251*, F904–F910. https://doi.org/10.1152/ajprenal.1986.251.5.f904.
6. Pietri, S.; Bernard, M.; Cozzone, P.J. Hydrodynamic and energetic aspects of exogenous free fatty acid perfusion in the isolated rat heart during high flow ischemia and reoxygenation: A ^{31}P magnetic resonance study. *Cardiovasc. Res.* **1991**, *25*, 398–406. https://doi.org/10.1093/cvr/25.5.398.
7. Durand, T.; Gallis, J.L.; Masson, S.; Cozzone, P.J.; Canioni, P. pH regulation in perfused rat liver: Respective role of $Na(^+)$-H^+ exchanger and $Na(^+)$-HCO_3^- cotransport. *Am. J. Physiol*. **1993**, *265*, G43–G50. https://doi.org/10.1152/ajpgi.1993.265.1.g43.
8. Khramtsov, V.V. Biological imaging and spectroscopy of pH. *Curr. Org. Chem*. **2005**, *9*, 909–923. https://doi.org/10.2174/1385272054038309.
9. Sapega, A.A.; Sokolow, D.P.; Graham, T.J.; Chance, B. Phosphorus nuclear magnetic resonance: A non-invasive technique for the study of muscle bioenergetics during exercise. *Med. Sci. Sports Exerc*. **1987**, *19*, 410–420. https://doi.org/10.1249/00005768-198708000-00015.
10. Roden, M. Non-invasive studies of glycogen metabolism in human skeletal muscle using nuclear magnetic resonance spectroscopy. *Curr. Opin. Clin. Nutr. Metab. Care* **2001**, *4*, 261–266. https://doi.org/10.1097/00075197-200107000-00003.
11. Foxall, P.J.; Nicholson, J.K. Nuclear magnetic resonance spectroscopy: A non-invasive probe of kidney metabolism and function. *Exp. Nephrol*. **1998**, *6*, 409–414. https://doi.org/10.1159/000020549.
12. Chapman, J.D. Measurement of tumor hypoxia by invasive and non-invasive procedures: A review of recent clinical studies. *Radiother. Oncol*. **1991**, *20*, 13–19. https://doi.org/10.1016/0167-8140(91)90181-f.
13. Mancuso, A.; Zhu, A.; Beardsley, N.J.; Gliskson, J.D.; Wehrli, S.; Pickup, S. Artificial tumor model suitable for monitoring ^{31}P and ^{13}C NMR spectroscopic changes during chemotherapy-induced apoptosis in human glioma cells. *Magn. Reson. Med*. **2005**, *54*, 67–78. https://doi.org/10.1002/mrm.20545.
14. Street, J.C.; Mahmood, U.; Ballon, D.; Alfieri, A.A.; Koutcher, J.A. ^{13}C and ^{31}P NMR investigation of effect of 6-aminonicotimnamide on metabolism of RIF-1 tumor cells in vitro. *J. Biol. Chem*. **1996**, *271*, 4114–4119. https://doi.org/10.1074/jbc.271.8.4113.
15. Bubnovskaya, L.; Mikhailenko, V.; Kovelskaya, A.; Osinsky, S. Bioenergetic status and hypoxia in Lewis lung carcinoma assessed by ^{31}P NMR spectroscopy: Correlation with tumor progression. *Exp. Oncol*. **2007**, *29*, 207–211.
16. Fan, K.; Zhang, M. Recent developments in the food quality detected by non-invasive nuclear magnetic resonance technology. *Crit. Rev. Food Sci. Nutr*. **2019**, *59*, 2202–2213. https://doi.org/10.1080/10408398.2018.1441124.
17. Hatzakis, E. Nuclear magnetic resonance (NMR) spectroscopy in food sciences: A comprehensive review. *Compr. Rev. Food Sci. Food Saf*. **2019**, *18*, 189–220. https://doi.org/10.1111/1541-4337.12408.
18. Cheng, C.H.; Balsandorj, Z.; Hao, Z.; Pan, L. High-precision measurement of pH in the full toothpaste using NMR chemical shift. *J. Magn. Reson*. **2020**, *317*, 106771. https://doi.org/10.1016/j.jmr.2020.106771.
19. Pietri, S.; Miollan, M.; Martel, S.; Le Moigne, F.; Blaive, B.; Culcasi, M. α- and β-Phosphorylated amines and pyrrolidines, a new class of low toxic highly sensitive ^{31}P NMR pH indicators. *J. Biol. Chem.* **2000**, *275*, 19505−19512. https://doi.org/10.1074/jbc.M001784200.
20. Lundberg, P.; Harmsen, E.; Ho, C.; Vogel, H.J. Nuclear magnetic resonance studies of cellular metabolism. *Anal. Biochem*. **1990**, *191*, 193−222. https://doi.org/10.1016/0003-2697(90)90210-z.
21. Satre, M.; Martin, J.B.; Klein, G. Methyl phosphonate as a ^{31}P-NMR probe for intracellular pH measurements in *Dictyostelium amoebae*. *Biochimie* **1989**, *71*, 941−948. https://doi.org/10.1016/0300-9084(89)90076-X .
22. Robitaille, P.M.L.; Robitaille, P.A.; Brown, G.G., Jr.; Brown, G.G. An analysis of the pH-dependent chemical-shift behavior of phosphorus-containing metabolites. *J. Magn. Reson*. **1991**, *92*, 73−84. https://doi.org/10.1016/0022-2364(91)90248-R.
23. Brénot, F.; Aubry, L.; Martin, J.B.; Satre, M.; Klein, G. Kinetics of endosomal acidification in *Dictyostelium discoideum* amoebae. ^{31}P-NMR evidence for a very acidic early endosomal compartment. *Biochimie* **1992**, *74*, 883–895. https://doi.org/10.1016/0300-9084(92)90072-M.
24. Raghunand, N.; Altbach, M.I.; van Sluis, R.; Baggett, B.; Taylor, C.W.; Bhujwalla, Z.M.; Gillies, R.J. Plasmalemmal pH-gradients in drug-sensitive and drug-resistant MCF-7 human breast carcinoma xenografts measured by ^{31}P magnetic resonance spectroscopy. *Biochem. Pharmacol*. **1999**, *57*, 309−312. https://doi.org/10.1016/s0006-2952(98)00306-2.

25. Lutz, N.W.; Le Fur, Y.; Chiche, J.; Pouysségur, J.; Cozzone, P.J. Quantitative in vivo characterization of intracellular and extracellular pH profiles in heterogeneous tumors: A novel method enabling multiparametric pH analysis. *Cancer Res*. **2013**, *73*, 4616−4628. https://doi.org/10.1158/0008-5472.can-13-0767.
26. Vidal, G.; Thiaudiere, E.; Canioni, P.; Gallis, J.L. Aminomethylphosphonate and 2-aminoethylphosphonate as ^{31}P-NMR pH markers for extracellular and cytosolic spaces in the isolated perfused rat liver. *NMR Biomed*. **2000**, *13*, 289–2996. https://doi.org/10.1002/1099-1492(200008)13:5%3C289::aid-nbm647%3E3.0.co;2-g.
27. Pietri, S.; Martel, S.; Culcasi, M.; Delmas-Beauvieux, M.C.; Canioni, P.; Gallis, J.L. Use of diethyl(2-methylpyrrolidin-2-yl)phosphonate as a highly sensitive extra- and intracellular ^{31}P NMR pH indicator in isolated organs. *J. Biol. Chem*. **2001**, *276*, 1750−1758. https://doi.org/10.1074/jbc.M008023200.
28. Martel, S.; Clément, J.L.; Muller, A.; Culcasi, M.; Pietri, S. Synthesis and ^{31}P NMR characterization of new low toxic highly sensitive pH probes designed for in vivo acidic pH studies. *Bioorg. Med. Chem*. **2002**, *10*, 1451−1458. https://doi.org/10.1016/s0968-0896(01)00414-x.
29. Gosset, G.; Satre, M.; Blaive, B.; Clément, J.L.; Martin, J.B.; Culcasi, M.; Pietri, S. Investigation of subcellular acidic compartments using α-aminophosphonate ^{31}P nuclear magnetic resonance probes. *Anal. Biochem*. **2008**, *380*, 184–194. https://doi.org/10.1016/j.ab.2008.05.052.
30. Gosset, G.; Martel, S.; Clément, J.L.; Blaive, B.; Olive, G.; Culcasi, M.; Rosas, R.; Thévand, A.; Pietri, S. Nouveaux marqueurs de pH utilisables en RMN du ^{31}P. Détermination de la relaxation longitudinale en fonction de la structure chimique, de la température, du pH et du milieu biologique. *CR Chim*. **2008**, *11*, 541–552. https://doi.org/10.1016/j.crci.2007.08.016.
31. Thétiot-Laurent, S.; Gosset, G.; Clément, J.-L.; Cassien, M.; Mercier, A.; Siri, D.; Gaudel-Siri, A.; Rockenbauer, A.; Culcasi, M.; Pietri, S. New amino-acid based β-phosphorylated nitroxides for probing acidic pH in biological systems by EPR spectroscopy. *ChemBioChem* **2017**, *18*, 300–315. https://doi.org/10.1002/cbic.201600550.
32. Culcasi, M.; Casano, G.; Lucchesi, C.; Mercier, A.; Clément, J.L.; Pique, V.; Michelet, L.; Krieger-Liszkay, A.; Robin, M.; Pietri, S. Synthesis and biological characterization of new aminophosphonates for mitochondrial pH determination by ^{31}P NMR spectroscopy. *J. Med. Chem*. **2013**, *56*, 2487–2499. https://doi.org/10.1021/jm301866e.
33. Culcasi, M.; Thétiot-Laurent, S.; Atteia, A.; Pietri, S. Mitochondrial, acidic, and cytosolic pHs determination by ^{31}P NMR spectroscopy: Design of new sensitive targeted pH probes. In *Mitochondrial Medicine: Methods in Molecular Biology*; Weissig, V., Edeas, M., Eds.; Humana Press: New York, NY, USA, 2015; Volume 1265, pp. 135–147. https://doi.org/10.1007/978-1-4939-2288-8_11.
34. Clarke, K.; Stewart, L.C.; Neubauer, S.; Balshi, J.A.; Smith, T.W.; Ingwall, J.S.; Nédélec, J.F.; Humphrey, S.M.; Kléber, A.G.; Springer, C.S., Jr. Extracellular volume and transsarcolemmal proton movement during ischemia and reperfusion: A ^{31}P NMR spectroscopic study of the isovolumic rat heart. *NMR Biomed*. **1993**, *6*, 278–286. https://doi.org/10.1002/nbm.1940060407.
35. Hunjan, S.; Mason, R.P.; Mehta, V.D.; Kulkarni, P.V.; Aravind, S.; Arora, V.; Antich, P.P. Simultaneous intracellular and extracellular pH measurement by ^{19}F NMR of 6-fluoropyridoxol. *Magn. Reson. Med*. **1998**, *39*, 551–556. https://doi.org/10.1002/mrm.1910390407.
36. Page, P.; Mazières, M.R.; Bellan, J.; Sanchez, M.; Chadret, B. A simple and convenient synthesis of 2-phosphonomethyl pyridines. *Phosphorus Sulfur Silicon Relat. Elem.* **1992**, *70*, 205–210. https://doi.org/10.1080/10426509208049168.
37. Ząd̨ło-Dobrowolska, A.; Kłossowski, S.; Koszelewski, D.; Paprocki, D.; Ostaszewski, R. EnzymaticUgi Reaction with Amines and CyclicImines. *Chem. Eur. J*. **2016**, *22*, 16684–16689. https://doi.org/10.1002/chem.201603412.
38. Pfafferott, G.; Oberhammer, H.; Boggs, J.E.; Caminati, W. Geometric structure and pseudorotational potential of pyrrolidine. An ab initio and electron diffraction study. *J. Am. Chem. Soc*. **1985**, *107*, 2305–2309. https://doi.org/10.1021/ja00294a017.
39. Gosset, G.; Clément, J.L.; Culcasi, M.; Rockenbauer, A.; Pietri, S. CyDEPMPOs: A class of stable cyclic DEPMPO derivatives with improved properties as mechanistics markers of stereoselective hydroxyl radical adduct formation in biological systems. *Biorg. Med. Chem.* **2011**, *19*, 2218–2230. https://doi.org/10.1016/j.bmc.2011.02.040.
40. Huck, V.; Niemeyer, A.; Goerge, T.; Schnaeker, E.M.; Ossig, R.; Rogge, P.; Schneider, M.F.; Oberleithner, H.; Schneider, S.W. Delay of acute intracellular pH recovery after acidosis decreases endothelial cell activation. *J. Cell Physiol*. **2007**, *211*, 399–409. https://doi.org/10.1002/jcp.20947.
41. Simchowitz, L.; Davis, A.O. Intracellular pH recovery from alkalinization. Characterization of chloride and bicarbonate transport by the anion exchange system of human neutrophils. *J. Gen. Physiol*. **1990**, *96*, 1037–1059. https://doi.org/10.1085/jgp.96.5.1037.
42. Ohta, K. Prediction of pKa values of alkylphosphonic acids. *Bull. Chem. Soc. Jpn.* **1992**, *65*, 2543–2545. https://doi.org/10.1246/bcsj.65.2543.
43. Lemercier, C. Nitroxydes β-Phosphorés et *n*-Alcoxyamines Dérivées en Polymérisation Radicalaire Contrôlée: Syntheses, Etudes Physico-Chimiques, Mécanismes. Ph.D. Thesis, Université d'Aix-Marseille I, Marseille, France, 2000.
44. Jencks, W.P.; Regenstein. J. Ionization constants of acids and bases. In *Handbook of Biochemistry and Molecular Biology*, 4th ed.; Lundblad, R.L., MacDonald, F.M., Eds.; CRC Press: Boca Raton, FL, USA, 2010; pp. 595–635; ISBN: 978-0-8493-9168-2.
45. Gosset, G. Nouvelles Sondes Phosphorées Adaptées à la Mesure du pH et du Stress Oxydant par RMN du ^{31}P et par RPE en Milieu Cellulaire. Ph.D. Thesis, Université d'Aix-Marseille I, Marseille, France, 2009.

46. Maurelli, E.; Culcasi, M.; Delmas-Beauvieux, M.C.; Miollan, M.; Gallis, J.L.; Tron, T.; Pietri, S. New perspectives on the cardioprotective phosphonate effect of the spin trap 5-(diethoxyphosphoryl)-5-methyl-1-pyrroline N-oxide: An hemodynamic and 31P NMR study in rat hearts. *Free Radic. Biol. Med*. **1999**, *27*, 34–41. http://doi.org/10.1016/s0891-5849(99)00033-7.
47. Delmas-Beauvieux, M.C.; Pietri, S.; Culcasi, M.; Leducq, N.; Valeins, H.; Liebgott, T.; Diolez, P.; Canioni, P.; Gallis, J.-L. Use of spin-traps during warm ischemia-reperfusion in rat liver: Comparative effect on energetic metabolism studied using ^{31}P nuclear magnetic resonance. *MAGMA* **1997**, *5*, 45–52. http://doi.org/10.1007/BF02592265.
48. Davies, L.; Farrar, N.A.; Satre, M.; Dottin, R.P.; Gross, J.D. Vacuolar H(+)–ATPase and weak base action in Dictyostelium. *Mol. Microbiol*. **1996**, *22*, 119–126. http://doi.org/10.1111/j.1365-2958.1996.tb02661.x.
49. Chalier, F.; Tordo, P. 5-Diisopropoxyphosphoryl-5-methyl-1-pyrroline *N*-oxide, DIPPMPO, a crystalline analog of the nitrone DEPMPO: Synthesis and spin trapping properties. *J. Chem. Soc. Perkin Trans.* **2002**, *2*, 2110–2117. https://doi.org/10.1039/B206909C.
50. Frisch, M.J.; Trucks, G.W.; Schlegel, H.B.; Scuseria, G.E.; Robb, M.A.; Cheeseman, J.R.; Scalmani, G.; Barone, V.; Petersson, G.A.; Nakatsuji, H.; et al. *Gaussian 16, Revision A.03*; Gaussian Inc.: Wallingford, CT, USA, 2016.
51. AMPAC 11, 1992–2017 Semichem, Inc. 12456 W 62nd Terrace—Suite D, Shawnee, KS 66216. Available online: http://www.semichem.com/ (assessed on 15 September 2019).
52. Tomasi, J.; Mennucci, B.; Cammi, R. Quantum mechanical continuum solvation models. *Chem. Rev*. **2005**, *105*, 2999–3093. https://doi.org/10.1021/cr9904009.
53. Cassien, M.; Petrocchi, C.; Thétiot-Laurent, S.; Robin, M.; Ricquebourg, E.; Kandouli, C.; Asteian, A.; Rockenbauer, A.; Mercier, A.; Culcasi, M.; et al. On the vasoprotective mechanisms underlying novel β-phosphorylated nitrones: Focus on free radical characterization, scavenging and NO-donation in a biological model of oxidative stress. *Eur. J. Med. Chem*. **2016**, *119*, 197–217. https://doi.org/10.1016/j.ejmech.2016.04.067.
54. Cassien, M.; Mercier, A.; Thétiot-Laurent, S.; Culcasi, M.; Ricquebourg, E.; Asteian, A.; Herbette, G.; Bianchini, J.-P.; Rahariv-elomanana, P.; Pietri, S. Improving the antioxidant properties of *Calophyllum inophyllum* seed oil from French Polynesia: Development and biological applications of resinous ethanol-soluble extracts. *Antioxidants* **2021**, *30*, 199. https://doi.org/10.3390/antiox10020199.
55. Kandouli, C.; Cassien, M.; Mercier, A.; Delehedde, C.; Ricquebourg, E.; Stocker, P.; Mekaouche, M.; Leulmi, Z.; Mechakra, A.; Thétiot-Laurent, S.; et al. Antidiabetic, antioxidant and anti-inflammatory properties of water and *n*-butanol soluble extracts from Saharian *Anvillea radiata* in high-fat-diet fed mice. *J. Ethnopharmacol*. **2017**, *207*, 251–267. https://doi.org/10.1016/j.jep.2017.06.042.